Leaching of trace metals (Pb) from contaminated tailings amended with iron oxides and manure: New insight from a modelling approach

Samuel Mertz, Lydie Le Forestier, Philippe Bataillard, Nicolas Devau

Journal Pre-proof

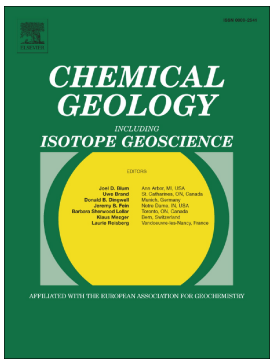

Leaching of trace metals (Pb) from contaminated tailings amended with iron oxides and manure: New insight from a modelling approach

Samuel Mertz, Lydie Le Forestier, Philippe Bataillard, Nicolas Devau

PII: S0009-2541(21)00300-4

DOI: https://doi.org/10.1016/j.chemgeo.2021.120356

Reference: CHEMGE 120356

To appear in: *Chemical Geology*

Received date: 8 October 2020

Revised date: 21 May 2021

Accepted date: 26 May 2021

Please cite this article as: S. Mertz, L. Le Forestier, P. Bataillard, et al., Leaching of trace metals (Pb) from contaminated tailings amended with iron oxides and manure: New insight from a modelling approach, *Chemical Geology* (2021), https://doi.org/10.1016/j.chemgeo.2021.120356

Leaching of trace metals (Pb) from contaminated tailings amended with iron oxides and manure: New insight from a modelling approach

Authors:

Samuel Mertz[ab], Lydie Le Forestier[ab*], Philippe Bataillard[b], Nicolas Devau[b]

[a] Univ. Orléans, CNRS, BRGM, ISTO, UMR 7327, F-45071, Orléans, France.

[b] BRGM, BP 36009, F-45060, Orléans, France.

Keywords: Lead, zinc, sorption, microbial respiration, dissolution, organic amendments.

ABSTRACT

Reclamation measurements are commonly applied to mitigate the leaching of metal pollutants in order to reduce the risk for humans and the environment. The stabilization of mine tailings can be performed by amending with organic or inorganic materials. In a recent laboratory microcosm experiment (Thouin et al., 2019), the addition of a mining slurry called ochre and manure, either alone or in combination, drastically reduced the leaching of several metal pollutants, notably Pb. Nevertheless, the biogeochemical processes involved in the immobilization of metal pollutants remain unknown, preventing the management of this remediation technique from being optimized and its extension to other sites. To fill this gap, a multicomponent mixing model was developed to simulate and forecast the impact of amendments on the leaching of metal pollutants. This model accounts for the following biogeochemical processes: kinetically-controlled dissolution/precipitation reactions, sorption

*Corresponding author.
E-mail address: lydie.leforestier@univ-orleans.fr (L. Le Forestier)

reactions (i.e. surface complexation reactions), water-gas interactions and microbial respiration with an explicit microbial growth. For all treatments, simulations revealed that Pb reactivity followed dynamic patterns driven by watering steps. The decrease in Pb concentration in the leachates of amended tailings compared to untreated tailings was also accurately reproduced. In untreated tailings, Pb reactivity is mainly controlled by the dissolution of Pb-bearing mineral phases. These reactions were maintained in thermodynamic disequilibrium due to the renewal of pore solution at each watering step. In amended tailings, this pattern was strengthened as the iron oxides contributed by ochre maintained a low Pb concentration in pore solution by sorbing released Pb. Sorption reactions were enhanced by the increase in pH induced by the dissolution of calcium carbonate initially present in ochre. The latter reaction was partially counterbalanced in tailings amended with manure as organic matter provided sufficient energy to fuel microbial aerobic respiration, leading to the release of protons. Pb desorption was promoted by this pH drop. The magnitude of these reactions was not strictly proportional to the amount of manure added. For 0.15% by weight, aerobic respiration did not occur whereas its yield was similar for 1% and 2%. By providing a better understanding of the effect of amendment, this multicomponent mixing model is a powerful tool to optimize the reclamation of tailings, in order to limit contaminant transfer to the environment.

1. Introduction

The anthropogenic contribution of metallic contaminants to the aquatic environment is not recent and dates back to the first mining activities, as attested by the 5000-year-old metal contaminations identified in the Rio Tinto in Spain (Davis Jr. et al., 2000). Europe was once a major mining region before witnessing a significant decline in mining activities in the late 20th century (Wolkersdorfer and Bowell, 2004). Consequently, abandoned mining sites are common in European countries and especially in France where the overall amount of tailings is estimated between 90 and 130 Mt (BRGM, 1997). Numerous studies have shown that

abandoned metallic mining sites can deteriorate water quality due to the mobilization of metal contaminants in response to the weathering of tailings (Akcil and Koldas, 2006; Gemici, 2008; Atanacković et al., 2013). This contamination can pose a health risk to residents living near mines (Lee et al., 2005; Park et al., 2014) and endangers the surrounding ecosystem (Sánchez-Chardi et al., 2007; Bori et al., 2016; Thienpont et al., 2016).

The oxidation of sulfide minerals initially present in tailings exposed to air and water has been identified as the main driver explaining the pollution of environmental compartments (groundwater, surface water and sediments) by metal contaminants. Following the oxidation of the primary mineral phases, metal contaminant carrier phases such as carbonate and/or sulfate minerals may be formed. Such conditions also lead to the precipitation of Fe- and Mn-oxides sorbing metal contaminants as emphasized by several authors (McCarty et al., 1998; Gemici, 2008). The occurrence, location and rate of the geochemical reactions are controlled by physical, chemical and biological properties of pore water and gaseous phase (Blowes and Jambor, 1990; Roussel et al., 2000). Previous studies have hinted that metal mobility in tailings is strongly controlled by the pH of pore water (Jurjovec et al., 2002; Jing et al., 2004; Al-Abed et al., 2008; Cappuyns et al., 2014). The mineralogical composition of the tailings directly influences the pH value of pore water. Silicate minerals, although having a greater overall buffering capacity in comparison to calcite per mole of mineral, exhibit a much slower dissolution, thus limiting their acid-neutralization capacity (Weber et al., 2005). Another important driver of the concentration of dissolved metals is microbial activity. Microorganisms can both immobilize metals by biosorption and reductive precipitation (McHale and McHale, 1994; Kashefi et al., 2001) and mobilize them by bioleaching and oxidative dissolution (Kelley and Tuovinen, 1988; Francis, 1990). In older mining sites, the mobilization of metal contaminants from tailings is therefore controlled by complex geochemical patterns in which secondary mineral phases may act as permanent or temporary source and sink terms. Metal contaminants are then often trapped in sulfated phases such as beudantite, anglesite, and plumbojarosite or carbonate phases such as cerussite (Courtin-Nomade et al., 2016).

In order to prevent the mobilization of metal contaminants in aged tailings, stabilization techniques based on using amendments have been developed and applied (Kumpiene et al., 2008). Amendments are inorganic or organic materials that are selected to prevent metal contaminants leaching during infiltration by modifying the physical, chemical and biological properties of tailings in order to enhance sorption, complexation or (co)-precipitation of metal contaminants. Furthermore, changes induced by amendments also limit tailings erosion by making plant growth easier. To date, the effects of various kinds of amendment to reduce divalent metal contaminants such as lead (Pb) or zinc (Zn) have been studied. Numerous studies have investigated the effect of biochar, an organic amendment made from biomass via pyrolysis, on aged tailings (Fellet et al., 2014; Nandillon et al., 2019; Norini et al., 2019; Lebrun et al., 2020). It is used to reduce soil acidity and nutrient leaching in order to promote the immobilization of metal contaminants and plant growth. Another possibility is to mix organic waste such as manure or slurry with marble wastes (Zornoza et al., 2013; Acosta et al., 2018). Organic wastes provide the nutrients necessary for plant growth, while marble wastes tend to increase pH, enhancing the immobilization of metal contaminants. To fully understand the influence of amendments on the behavior of metal contaminants, Thouin et al. (2019) set up an original leaching experiment on mine tailings configured to be close to real conditions. The dynamic of natural recharge was reproduced by a regular water supply (every week). This protocol better represents natural conditions, in which the pore water is renewed frequently. The experiment took place over a long period (3 months) in order to better represent the evolution of the system. Leaching was performed on aged mine tailings with or without amendments. When the tailing was not amended, a high Pb concentration was measured in the leachate, mainly caused by acid conditions. The amendments chosen had the advantage of being available near the site. Unlike most studies using only carbonates as amendments to reduce the leaching of metal contaminants, the first amendment used was a sludge called ochre produced from a coal mine water treatment plant. It was mainly composed of iron oxy-hydroxides associated with aragonite. The main effect generated by this amendment was to increase the pH, but also to enhance the sorption

capacity of the tailing, leading to a significant drop in the Pb concentration. The second amendment used was cow manure: this addition is necessary to allow plant growth on the residue, mixed with ochre. Similar results to those obtained with the ochre alone were observed with this mixed amendment. Apart from a slight increase in Pb concentration during the first half of the experiment, a decrease to the base level during the rest of the experiment was recorded. Therefore, Thouin et al. (2019) identified promising amendments to reduce Pb mobility in contaminated tailings. Nevertheless, this experiment, though critical for understanding these systems, was essentially qualitative as the nature and the rate of the main biogeochemical processes involved in the immobilization of Pb remain unknown.

A quantitative evaluation of metal contaminant mobility in tailings requires using multicomponent reactive transport models. While these tools have largely helped to determine the relative part of various geochemical processes taking place in tailings, they have been mainly devoted to simulating dissolution rates of sulfides under oxidizing conditions and the associated biogeochemical reactions such as the microbially-driven Fe(II)-oxidation reaction, precipitation of sulfate and carbonate minerals or O_2 diffusion in gaseous and aqueous phases (Gerke et al., 2001, 1998; Mayer et al., 2002). By contrast, they have been less used to simulate the mobility of metal contaminants in aged tailings or to estimate the effects of amendments. The first studies that modelled the behaviour of metal contaminants in aged tailings were based on the assumption of thermodynamic reaction control (Harwood and Kotyohann, 1987; Walter et al., 1994), or used simplified kinetic laws such as zero/first-order dissolution rate laws (Eriksson and Destouni, 1997). More recent studies have highlighted a better prediction of metal release in pore water, describing the kinetic dissolution of minerals mechanistically, but some important geochemical processes such as sorption reactions were not taken into account in the simulations (Acero et al., 2009; Ouangrawa et al., 2009; Pabst et al., 2017).

The objective of the present study was to identify and prioritize the nature and the rate of the physical processes and biogeochemical reactions controlling the mobility of dissolved metal contaminants in aged tailings that are stabilized by amendments. To tackle

this goal, a multicomponent mixing transport model was built to simulate and predict the results of the leaching experiments done in Thouin et al. (2019). Different biogeochemical processes were explored during the model building in order to describe the experimental data and provide new insight on the reactivity of metal contaminants. The main pollutant targeted by the model was Pb, which was the principal pollutant identified in the tailings. Simulations of several chemical properties of leachates were also conducted (Zn, SO_4^{2-} and Ca concentrations as well as pH values). Experimental results obtained for untreated tailings were simulated first. Then, the model was applied to the tailings amended with ochre alone or in association with cow manure.

2. Methods

2.1 Mine tailings

Tailings were sampled at a former mine exploiting Pb and Ag named Roure-les-Rosiers (Puy de Dôme, France, 45°47'29''N 2°49'18''E), a part of the Pontgibaud mining district. It has been exploited since antiquity with a peak of activity in the 19th century before closing in 1901. Granulometric analysis indicated that the tailings were mainly composed of sand (>90%) with a low silt-clay fraction. These tailings had a very low organic matter content, with only 0.09% of total organic carbon measured by Rock-Eval pyrolysis (Thouin et al., 2019).In order to get as much information as possible on the mineralogical assemblage, X-ray diffractograms (XRD) in Thouin et al. (2019) have been interpreted with more caution to assess the mineral phases present in the tailings in order to strengthen the hypotheses underlying the geochemical model. The XRD revealed the main presence of quartz and feldspar, i.e. mineral phases having low interactions with metal contaminants (Fig. A.7). A phyllosilicate has been detected which appears to be muscovite. Sulfated Pb-bearing phases were also identified: anglesite $PbSO_4$ and beudantite $PbFe_3(AsO_4)(SO_4)(OH)_6$, a solid

solution between plumbojarosite $Pb_{0.5}Fe_3(SO_4)_2(OH)_6$ and segnitite $PbFe_3H(AsO_4)_2(OH)_6$. Chlorine phases such as pyromorphite were not detected.

2.2 Leaching experiment

Only a brief description of the leaching experiment is given here; further details can be found in Thouin et al. (2019). Leaching tests at a microcosm scale were performed on tailing samples to simulate the percolation of rainwater. Different additions of amendments were applied to evaluate their effects on the mobility of metal contaminants. The first amendment used was a mining slurry called ochre. As for mine tailings, a more detailed interpretation of XRD done by Thouin et al. (2019) revealed the presence of several crystalline phases, namely iron(III) oxide-hydroxide (goethite) and aragonite (Fig. A.7). The large peaks of goethite suggest a poorly crystalline goethite. Zincite is suspected here, a small peak at 2.476 Å between those of aragonite and goethite can be attributed to zincite. The second amendment used was cow manure, as this type of organic amendment can improve the agronomic properties of the tailings in order to facilitate vegetation growth (Sumner, 2000). The only crystalline phase identified in cow manure was quartz (Fig. A.7). The leaching tests were carried out in polystyrene pots (5 cm diameter, 10 cm height) of which the bottoms were perforated to allow the flow of leaching water (Fig. A.1). A thin layer of glass wool covered with sand (Fontainebleau) was laid at the bottom of the pot to retain the soil particles. A mass of 150 g of residues, previously dried and sieved at 2 mm, was used for each leaching test. The mineral water (Mount Roucous) was chosen for leaching because its chemical composition is similar to that of rainwater (Table 1). The leaching experiments extended over a period of 3 months (84 days) with leaching of 25 mL every 7 days (i.e. 13 leaching steps). The different conditions tested were as follows: without amendment (T), with 5 wt% ochre (TO), with 5wt% ochre and 0.15, 1 or 2wt% manure (TOM 0.15, TOM 1 and TOM 2, respectively). Pb and pH were measured every week and more complete geochemical analyses (Zn, Ca, Na, K, Cl, Mg, Li, Br, SO_4^{2-}, NO_3^-, NH_4^+) were

performed three times (7, 35 and 84 days). Chemical analyses were performed on solution filtered at 0.45 µm, and the pH was also measured (Thouin et al., 2019). Pb, Ba and As were analyzed by oven AAS (Varian spectrAA) and Zn by flame AAS (Varian spectrAA). An ion chromatography (IC) using a 940 Professional IC Vario instrument (Metrohm) equipped with conductivity detectors was employed to quantify major ions (Li^+, Na^+, NH_4^+, K^+, Ca^{2+}, Mg^{2+}, Cl^-, Br^-, NO_3^-, SO_4^{2-}).

Table 1

Chemical composition of the mineral water (Mont Roucous) and the initial pore water of the tailing alone used for each simulation.

	pH	SO_4^{2-} (mol L^{-1})	Pb (mol L^{-1})	Zn (mol L^{-1})	Ca (mol L^{-1})
Mineral water	6	3.2×10^{-5}	--	--	7.2×10^{-5}
Tailing	6	4.6×10^{-4}	4.3×10^{-5}	7.9×10^{-6}	4×10^{-4}[a]
Tailing + Amendment[b]	7.7	1.8×10^{-2}	1.9×10^{-7}	1.1×10^{-6}	3×10^{-2}

[a] Modified concentration to obtain a saturation index close to the thermodynamic equilibrium for the minerals initially present in the tailings.

[b] Similar pore water composition for Tailing + Ochre and Tailing + Ochre + Manure.

2.3 Multicomponent mixing model

All the numerical simulations were performed using the geochemical PHREEQC code (Parkhurst and Appelo, 2013). The multicomponent mixing transport model was built by using this code, taking transport in aqueous phase and gaseous phase and several geochemical reactions into account. A mixing framework was used to mimic transport. The following geochemical reactions were included in the model: thermo-kinetically-controlled dissolution or precipitation reactions for the primary and secondary mineral phases, surface complexation reactions onto iron oxides and organic matter, and microbial respiration. Most of the thermodynamic data used in the model were taken from the well-known Thermoddem database (Blanc et al., 2012). Unfortunately, no value was referenced for some model

parameters. To overcome this gap, these values were calibrated according to measured data. The PEST (Parameter ESTimation) software (Doherty, 2015) was used to assess the uncertainty of the model parameters. The software has been widely used for parameter estimation, sensibility analysis and can be easily coupled with PHREEQC. In order to estimate the value of each parameter, PEST uses the Gauss-Marquardt-Levenberg method based on the comparison between the simulated and observed output variable values. More details on the specificities of the model are given below.

2.3.1. Initial conditions

The mineralogical assemblage and initial pore solution used in the simulations were first determined for the untreated tailings. These model parameters were then updated in order to account for amendment, either by ochre (TO) or by ochre plus manure (TOM). Assumptions were made based on the previous investigation by Thouin et al. (2019), using chemical analysis on solid phases and re-interpreted XRD analysis made on the tailings and the amendments. For each treatment, an appropriate framework was developed to estimate the chemical composition of the initial pore solution as no measurements were available, except for pH value and Pb concentration.

In untreated tailings, two main Pb-bearing mineral phases were detected through XRD, anglesite and beudantite. These mineral phases were also observed by Pascaud et al. (2014) in the tailings of the Pontgibaud mine, located about 7 km to the northeast from our site. Beudantite forms a solid-solution between plumbojarosite (sulfate end-member) and segnitite (arseniate end-member). The end-member used in the model was chosen on the basis of its capacity to simulate the reactivity of the main contaminant, namely Pb and the evolution of pH. These parameters were correctly described with plumbojarosite and so depend on this phase. The concentrations of these two phases were fixed using Pb and SO_4^{2-} concentrations measured in the tailing. However, the proportion of these two phases was optimized due to a lack of information about their relative abundance. XRD

measurements revealed the presence of feldspar in the tailings. The diffractograms suggest the existence of K-feldspar but other types of feldspar are likely to be present in lesser quantities. A small amount (0.1 wt%) of anorthite, being in adequacy with the measurements of CaO carried out on the tailings (Thouin et al., 2019), was considered in the simulation to describe the reactivity of Ca. The chemical investigation performed on the solid phase revealed that iron oxides were present in the initial material. The absence of detection in XRD measurements suggests a low relative amount i.e. < 5wt%. We assumed that these iron oxides correspond to ferrihydrite in the simulations. Not all the Fe was attributed to ferrihydrite (5%), because other mineral phases may contain it, in particular plumbojarosite. In order to identify Zn sources in the tailings the saturation index (SI) calculations were established with the chemical composition of the leachate. These calculations have shown that all the Zn-bearing phases listed in the Thermoddem database are far from equilibrium, suggesting that no Zn-bearing phase is present in the tailings. It has been shown that divalent metals such as Zn have the ability to replace Pb present in plumbojarosite (Dutrizac, 1984) by substitution in environments highly polluted with Zn and in low amounts (< 4wt%). Low Zn concentrations have also been reported in anglesite (Bril et al., 2008) in a Zn-smelting slag context. Therefore, in order to correctly describe the dynamics of Zn in the system and to respect the measurements of total Zn performed in the tailings, a small amount of Zn was assumed to be present in plumbojarosite and in anglesite with the following ratios, 0.5wt% and 0.4wt% respectively. To confirm our assumption, XRD results issued from Thouin et al. (2019) have been interpreted to identify whether Zn-bearing crystalline phases are present in the mineralogical assemblage (Fig. A.7). To simplify the model, Zn trapping in solid phase was considered with anglesite precipitation as we assumed that dissolution and precipitation reactions are identic in term of stoichiometry in our simulations. No Zn-bearing crystalline phase was detected. This absence of detection could confirm our hypothesis. Nevertheless, this result should be taken with caution as it could also indicate that the amount of Zn-bearing crystalline phases is low in tailings or amorphous phase could be present. To be sure that no Zn-bearing phases is present in the tailings,

more sophisticated spectrometry techniques such as extended X-ray absorption fine structure or the electron dispersive X-ray spectrometry within a scanning electron microprobe should be used. This mineralogical assemblage was used to calculate the chemical composition of the initial pore solution (Table 2). We assumed the pore solution was in thermodynamic equilibrium with the mineralogical assemblage at the beginning of the leaching experiment. The lack of additional information on the composition of the mineralogical phase prevented us from simulating the dynamics of other elements than those controlled by the phases observed in the tailing (Pb, SO_4^{2-}, Ca and Zn). While one can associate each concentration of these element with a particular phase, in our simulations each of the solution parameters is highly dependent on several geochemical processes as we used a multi-component model in the present study. This model is based on physical laws, implying mass balance and thermodynamic laws.

To calculate the mineralogical assemblage considered to simulate leaching in tailing amended with ochre (TO), we first analysed the mineralogical assemblage of ochre based on the chemical analysis and XRD analysis done on this material. These measurements revealed that ochre, a by-product of coal mine water, exhibited a high Fe content, suggesting the presence of a large amount of iron oxides. X-ray diffractograms revealed the presence of poorly crystalline goethite (Fig. A.7). The surface area used for this phase in our simulations was 200 $m^2\ g^{-1}$, which is higher than the surface areas commonly measured in well crystallized goethite and corresponds to a poorly crystalline phase. In order to keep a continuity between the different simulations and to simplify the model, only one of iron oxy-hydroxide phase was considered in the simulations, namely ferrihydrite. The amount of ferrihydrite contributed by ochre was calculated by assuming that all Fe present in solid phase was allocated to this mineral phase. Due to the significant amount of Zn in ochre (21,830 mg kg^{-1}, Thouin et al., 2019), Zn-bearing phases were suspected to be present. Zincite was not clearly identified by XRD but doubts may remain due to the small peak observed at 2.4759 Å. We therefore assumed that Zn was provided by ochre *via* zincite. The amount of zincite in ochre mineral phase was calculated by assuming that all the Zn

measured in solid phase was allocated to this mineral phase. This represents a small proportion of the ochre (2 wt%), which could explain the difficulty in identifying zincite via XRD.

The leachates obtained in tailing amended with ochre 7 days after the beginning of the experiment exhibited high Ca and SO_4^{2-} concentrations (see below). XRD revealed the presence of aragonite as Ca-bearing phase (Fig. A.7). The amount of aragonite in ochre was then fixed using the concentration of inorganic carbon measured in the solid phase. However, no sulfated phase was recorded by XRD analysis. SI calculations made with the chemical composition of the leachate showed that calcium sulfates were close to thermodynamic equilibrium: gypsum (0.08), anhydrite (-0.09) and bassanite (-0.60). Measurement of total sulfur using an elemental pyrolyser analyzer (Flash 2000, Thermo Fischer Scientific) has indicated a concentration of 0.69 wt% (Thouin et al., 2019). As ochre is produced under oxic conditions, one can assume that the total sulfur detected in the solid phase is under oxidized state. This latter result indicates that the amount of sulfate in ochre is relatively low. We assume that this low concentration prevented the identification of these crystalline sulfate phases by XRD. In order to correctly describe the reactivity of SO_4^{2-}, gypsum was introduced in our simulations to represent this calcium sulfate. The log K of the reaction was modified to account for this unknown calcium sulfate and in order to better describe SO_4^{2-} reactivity (Table 2). The amount of gypsum present in the ochre was estimated according to the total S measurements, i.e. 0.69 wt%. These calculations were used to update the mineralogical assemblage calculated for untreated tailings. An adapted framework was used to assess the chemical composition of the initial pore solution. The new mineralogical assemblage (tailing + ochre) was put in contact for 3 days with the initial pore water of the tailing alone, before the start of the experiment. These conditions correspond to the experimental protocol of Thouin et al. (2019). As the newly added phases were not in thermodynamic equilibrium with the pore solution, the chemical composition of the pore water will evolve towards thermodynamic equilibrium during this time period.

The third treatment (TOM) corresponded to the addition of manure in variable proportions (0.15, 1 and 2wt%) and of 5wt% of ochre. Organic matter provided by manure can be dissolved, releasing organic carbon in solution. The organic carbon concentration in manure was measured by Rock-Eval pyrolysis (Thouin et al., 2019). This value was reported in our simulations where 0.065g, 0.43g and 0.86g of organic carbon was used for 0.15, 1 and 2wt% manure respectively. In order to assess the influence of microbial activity on the mobility of metals, microbial biomass was taken into account. The initial microbial biomass values for each proportion were estimated using DNA analysis (Thouin et al., 2019) and the microbial growth is then explicitly described (see below). The same framework as the one used for the second condition (TO) was chosen to estimate the chemical composition of the initial pore solution (Table 2). This new mineralogical assemblage (ochre + manure) was then brought into contact for 3 days with the initial pore water of the tailing alone. In order to assess the sensitivity of the model, an uncertainty analysis was carried out on the surface areas of anglesite and plumbojarosite (Table 2). These parameters are the fitted parameters controlling the most the system. The parameter's lower and upper bound were of an order of magnitude compared to the initial fitted value. This analysis was run for the simulation with tailings only (T) then for the simulations TO and TOM with 1% of manure.

Table 2

Mineralogical assemblage used for numerical modelling.

T: tailings without amendment, TO: tailings with ochre, TOM: tailings with ochre and manure.

Minerals	Reaction	Log K	T		TO		TOM (0.15/1/2wt%)	
			Amount (wt%)	SSA[b,d] ($m^2\ g^{-1}$)	Amount (wt%)	SSA[b,d] ($m^2\ g^{-1}$)	Amount (wt%)	SSA[b,d] ($m^2\ g^{-1}$)
Anorthite	$Ca(Al_2Si_2)O_8 + 8H^+ \leftrightharpoons 2Al^{3+} + Ca^{2+} + 2H_4SiO_4$	24.224[a]	0.1[b]	0.014	0.1[b]	0.014	0.1[b]	0.014
Aragonite	$CaCO_3 + H^+ \leftrightharpoons HCO_3^- + Ca^{2+}$	2.014[a]	--	--	0.5[c]	7×10^{-4}	0.5[c]	7×10^{-4}
Gypsum	$CaSO_4 \cdot 2H_2O \leftrightharpoons Ca^{2+} + SO_4^{2-} + 2H_2O$	-4.25[b]	--	--	0.2[c]	0.5	0.2[c]	0.5
Anglesite	$Pb_{0.98}Zn_{0.02}SO_4 \leftrightharpoons 0.98Pb^{2+} + 0.02Zn + SO_4^{2-}$	-7.848[a]	3.25[c]	3×10^{-2e} (2.99×10^{-2L} - 3.01×10^{-2u})	3.25[c]	1×10^{-3e} (0.84×10^{-3L} - 1.21×10^{-3u})	3.25[c]	1×10^{-3e} (0.84×10^{-3L} - 1.21×10^{-3u})

Plumbojarosite	$Pb_{0.455}Zn_{0.045}Fe_3(SO_4)_2(OH)_6 + 6H^+ \leftrightharpoons 3Fe^{3+} + 0.455Pb^{2+} + 2SO_4^{2-} + 6H_2O + 0.045Zn^{2+}$	11.456[a]	1.4[c]	7.2×10^{-2e} (7.19×10^{-2L} - 7.21×10^{-2u})	1.4[c]	9.2×10^{-3e} (8.45×10^{-3L} - 1×10^{-2u})	1.4[c]	9.2×10^{-3e} (8.45×10^{-3L} - 1×10^{-2u})
Ferrihydrite	$Fe(OH)_3 + 3H^+ \leftrightharpoons Fe^{3+} + 3H_2O$	3.399[a]	0.1[c]	40	3.6[c]	200	3.6[c]	200
Zincite	$ZnO + 2H^+ \leftrightharpoons Zn^{2+} + H_2O$	11.206[a]	--	--	0.13[c]	10	0.13[c]	5

[a] K values from Thermoddem database (Blanc et al., 2012)

[b] Fitted values.

[c] Estimated values using chemical analysis.

[d] SSA = Specific Surface Area

[e] Optimized values with PEST

[u] Upper bound of the 95% confidence limits

[L] Lower bound of the 95% confidence limits

2.3.2. Boundary conditions

No measurement of the advective flow was recorded during the experiments, preventing the description of the transport processes. Thus, several hypotheses were formulated in order to establish a simplified transport model. Firstly, the displacement of the water in the column was considered to be the result of a piston effect, where the pore water was replaced by the leaching water. Then at each leaching step, a mix was considered with a ratio of 90% leaching water to 10% pore water. After mixing, we assumed that the system remained closed until the next leaching step.

For the first two treatments without organic matter (T and TO), the solution was considered to be in equilibrium with respect to the atmosphere. Due to microbial activity this boundary condition was changed for the third treatment with organic matter (TOM). In order to have a finer description of water-gas exchanges, the solution was brought into contact with a fixed volume of gas without forcing the equilibrium. A mix between the soil gases and the atmosphere was carried out at each step, described as:

$$pCO_{2_{mix}} = f \cdot pCO_{2_{soil}} + (1 - f) \cdot pCO_{2_{atm}} \quad (1)$$

where $pCO_{2_{mix}}$ is the partial pressure of CO_2 obtained after the conservative mixture, f corresponds to the soil fraction CO_2 in the mix with atmosphere with the value of 0.75, $pCO_{2_{soil}}$ is the partial pressure of CO_2 in the soil and $pCO_{2_{atm}}$ corresponds to the partial pressure of CO_2 of the atmosphere (346 ppm).

2.4 Sorption

2.4.1 Iron oxides

Sorption reactions on iron oxides were simulated using the model of Dzombak and Morel (1990), which is based on the generalized two-layer model. This model takes into account both contributions allowing the sorption of cations and anions on the oxide surface, as well as their protonation: (i) the chemical contribution induced by the bond formation between the ion and the atoms present on the surface, and (ii) the electrostatic contribution induced by the surface charge. The equilibrium constant of the complexation reaction is defined as:

$$K = e^{\left(\frac{-\Delta G^{\circ}}{RT}\right)} \quad (2)$$

where ΔG° is the standard state free energy of the complexation reaction (J.mol^{-1}), T the temperature (K) and R the gas constant (8.31 J.K^{-1}.mol^{-1}). The protonation and deprotonation reactions at the ferrihydrite surface are shown in Table A.1. The sorption of three elements (Pb, Zn, Ca) was taken into account in the simulations (Table A.2). It follows a general equation for surface complexation:

$$S^{z_s}(A_i^{z_i})_{v_i} + v_j A_j^{z_j} = S^{z_s}(A_j^{z_j})_{v_j} + v_i A_i^{z_i} \quad (3)$$

where S is the chemical formula of a surface species, z the charge of a species, $A_{i,j}$ the chemical formulae of the sorbate species and $v_{i,j}$ are stoichiometric coefficients.

2.4.2 Organic matter

Sorption on organic matter can be modeled using WHAM (Windermere Humic Aqueous Model) (Tipping and Hurley, 1992). This model describes the sorption of protons and cations on humic acids via monodentate and bidendate binding sites. The electrostatic term of the reaction follows the theory of the electrical double-layer. The specific surface area (SSA) of humic acids is linked to the ionic strength of the solution according to an empirical relationship (Appelo and Postma, 2005). For a mean ionic strength of 0.02 M during the third treatment (TOM), the calculated SSA was about 26,300 $m^2\ g^{-1}$. Humic acid has a total charge of -7.1 meq g^{-1} in the WHAM model, which is distributed over eight monodentate sites and twelve bidentate sites. Monodentate sites are composed of four carboxylic sites (nHA carrying a charge of -2.84 meq g^{-1} humic acid) and four phenolic sites (nHB, charge = -1.42 meq g^{-1} humic acid) while bidendate sites combine carboxylic and phenolic charges (charge = -2.84 meq g^{-1} humic acid). The complexation parameters for protons and cations used in the simulation are indicated in Table A.3. The sorption of Pb, Zn and Ca follows this general formula:

$$H_{(a,\ldots,h)H} + Me^{2+} \rightleftharpoons H_{(a,\ldots,h)Me^{+}} + H^{+} \quad (4)$$

$$H_{(af,\ldots,dg)H} + Me^{2+} \rightleftharpoons H_{(af,\ldots,dg)Me^{+}} + H^{+} \quad (5)$$

2.5 Dissolution and precipitation

In order to model the dissolution and precipitation of the mineral phases a general transition-state-theory (TST) derived rate law (Lasaga, 1981 and 1984) was used :

$$\frac{dm}{dt} = -A \cdot \sum_{j} \left[k_j e^{\frac{-E_j}{R}\left(\frac{1}{T}-\frac{1}{298.15}\right)} f_j\left(a_{i,j}\right) g_j(\Delta G_r) \right] \quad (6)$$

where the rate $\frac{dm}{dt}$ is in mol s^{-1}, A is the surface area of the mineral (m^2), k is the reaction rate (mol $m^{-2}\ s^{-1}$), E_j is the activation energy (J mol^{-1}), R is the gas constant (J $mol^{-1}\ K^{-1}$) and T is the temperature (K). The term $f_j\left(a_{i,j}\right)$ is dimensionless and represents the activity of the i^{th}

aqueous species participating in the j[th] mechanism. For a single mechanism this term becomes:

$$f(a_i) = \prod_i a_i^{n_i} \quad (7)$$

where n_i is the reaction order of the i[th] aqueous species. The reaction order n_i is a value which reflects the influence of a species (H^+, OH^-, CO_2, ...) in the overall rate reaction. The term $g_j(\Delta G_r)$ is also dimensionless and takes into account the distance from equilibrium; the reaction rate will be slower near equilibrium. For a single mechanism:

$$g(\Delta G_r) = \left(1 - \frac{Q}{K}\right) \quad (8)$$

where *Q* is the activity product and *K* the equilibrium constant, then the ratio *Q/K* represents the mineral saturation index. For most minerals, up to 3 mechanisms will control their dynamics, namely those catalyzed by H^+ (acid mechanism), those catalyzed by OH^- (base mechanism), and those taking place in neutral conditions (neutral mechanism). The kinetic parameters used for each mineral phase are listed in Table 3. The precipitation rate constant was derived from the dissolution rate constant considering that precipitation is slower than dissolution.

Table 3

Kinetic parameters used to describe dissolution and precipitation of mineral phases in the simulation

Minerals	Kinetic parameters										
	Acid mechanism				Neutral mechanism			Base mechanism			
	k_{diss}[a]	k_{pre}[b]	E[c]	n[h]	k_{diss}[a]	k_{pre}[b]	E[c]	k_{diss}[a]	k_{pre}[b]	E[c]	n
Anorthite[e]	3.16×10^{-4}	3.16×10^{-5}	16.6	1.41	7.58×10^{-10}	7.58×10^{-11}	17.8	--	--	--	--
Aragonite[f]	0.5	0.05	14.4	1	1.54×10^{-6}	1.54×10^{-7}	23.5	3.3×10^{-4}	3.3×10^{-5}	35.4	1[i]
Gypsum[g]	--	--	--	--	1.62×10^{-3}	1.62×10^{-4}	0	--	--	--	--
Anglesite	1×10^{-7}*	8×10^{-8}*	31.3[d]	0.3[d]	8×10^{-9}*	6×10^{-9}*	31.3[d]	--	--	--	--
Plumbojarosite*	3×10^{-5}	$3. \times 10^{-6}$	79	0.89	2×10^{-6}	2×10^{-7}	79	1.1×10^{-10}	1.1×10^{-12}	79	0.39[j]
Ferrihydrite*	--	--	--	--	4×10^{-10}	4×10^{-11}	86.5	--	--	--	--

Zincite*	--	--	--	--	4×10^{-11}	4×10^{-12}	32	--	--	--	--

[a] Dissolution rate constant k_{diss} in mol m^{-2} s^{-1}

[b] Precipitation rate constant k_{pre} in mol m^{-2} s^{-1}

[c] Arrhenius activation energy E in kJ mol^{-1}

[d] Values from Dove and Czank, 1995

[e] Values from Palandri and Kharaka, 2004

[f] Considering parameters similar to calcite from Plummer et al., 1978

[g] Values from Raines and Dewers, 1997

[h] Reaction order n with respect to H^+

[i] Reaction order n with respect to pCO_2

[j] Reaction order n with respect to OH^-

* Fitted values

2.6 Microbial Respiration

In natural systems redox reactions are often catalyzed by microbial activity. Respiring microorganisms use some of the released energy for their growth by synthesizing adenosine triphosphate (ATP) from adenosine diphosphate (ADP) (Jin and Bethke, 2002 and 2003). The microbial respiration was then taken into account for the simulations, with organic carbon as electron donor and dioxygen as electron acceptor, according to the reaction:

$$H_2O + C_{org} + O_2 \leftrightharpoons CO_2 + H_2O \quad (9)$$

with Log K = 67.84. The value was obtained by calculating the Gibbs free energy of the reaction, using the standard Gibbs free energy of formation from Lange's Handbook of Chemistry (Dean, 1999), considering O_2 and C_{org} with $\Delta G_f = 0$. To describe the kinetic of this microbial respiration reaction, a model based on Monod's formalism with a thermodynamic factor was used. The rate *r* (mol L^{-1} s^{-1}) of the reaction is then expressed as:

$$r = k[X]F_D F_A F_T \quad (10)$$

where k is the rate constant (mol g^{-1} s^{-1}), $[X]$ is the biomass concentration (g L^{-1}), F_D and F_A are dimensionless kinetic factors accounting for concentration of chemical species involved in half redox reactions, and F_T is the thermodynamic potential factor. Kinetic factors are defined as:

$$F_D = \frac{[D]}{[D] + K_D} \quad (11)$$

$$F_A = \frac{[A]}{[A] + K_A} \quad (12)$$

where $[D]$ and $[A]$ are the concentration of the donor and the acceptor species (mol L^{-1}), respectively, and K_D and K_A the half-saturation constants (mol L^{-1}). The thermodynamic factor accounts for the effect of the thermodynamic driving force and can be described as:

$$F_T = 1 - \frac{Q}{K} \quad (13)$$

where *Q* is the activity product and *K* the equilibrium constant of the reaction. The parameters used for the Eq. 10 are k = 7 x 10^{-7} mol g^{-1} s^{-1}, K_D = 3 x 10^{-9} M and K_A = 3 x 10^{-9} M. A linear rate law describes the solubilisation of organic carbon:

$$r = k(C_t - C_i) \quad (14)$$

where k is the rate constant (s^{-1}), with a value of 6 x 10^{-7}, C_t is the total organic carbon quantity (mol) and C_i is the insoluble organic carbon quantity (mol). The C_t value was measured in manure, while the C_i value was fitted. Biomass evolution is explicitly described with a Monod rate expression as:

$$r_{bio} = -Yr - b[X] \quad (15)$$

where r_{bio} is the rate of biomass growth (g L^{-1} s^{-1}), *Y* is the microbial yield coefficient (g mol^{-1}) and *b* is the first-order biomass decay coefficient (s^{-1}). In this simulation *Y* = 0.5 g mol^{-1} and *b* = 10^{-7} s^{-1} .The biomass concentrations used at the start of the simulations correspond to those measured via DNA analyses 7 days after the start of the experiment. For 0.15, 1 and 2wt% manure, the biomass concentration was 7.7 x 10^{-3}, 2.2 x 10^{-2} and 5.5 x 10^{-2} g.L^{-1} respectively.

2.7 Model performance criteria

The Normalized Root Mean Square Error (NRMSE) was used to compare the model prediction and the measured values:

$$NRMSE = \frac{\sqrt{\frac{1}{n}\sum_{i=1}^{n}(p_i - m_i)^2}}{y} \quad (16)$$

where n is the number of observations, p_i the predicted values, m_i the measured values and y the mean value of the measured data. The closer the value of NRMSE is to 0, the better the model prediction is. This method still has a limitation as the comparison between the model and the data can only be done at the end of each leaching period, i.e. 7 days. However, NRMSE is a metric that provides for one parameter the overall goodness-of-fit in a time series. This method is therefore less sensitive to detect punctual discrepancy for a whole time series between modelling and experimental results. (Doherty, 2015).

3. Results and discussion

3.1 Tailings without amendment (T)

The modeled evolution of the Pb concentration in the leachate was compared to the measured values in Fig. 1.a. The model made it possible to properly fit the data (NRMSE = 5.2%). During the experiment, the Pb concentration measured in the leachate remained constant around the high value of 6.5 x 10^{-5} M, except for the first leaching step where Pb concentration increased from 4.5 x 10^{-5} M to 6.5 x 10^{-5} M. In the simulation, the initial Pb concentration of 4 x 10^{-5} M increased rapidly, reaching the maximum value of 2.4 x 10^{-4} M after 50 minutes. Pb concentration then decreased sharply over the next 9 hours, leading to a concentration more than 2 times lower (9 x 10^{-5} M). This decrease continued at a slower rate until the next watering (7 days after the start of the experiment), Pb concentration being

lowered by 32% (6.1 x 10^{-5} M). Immediately after watering, Pb concentration dropped to 3.9 x 10^{-5} M, before increasing by 150% (9.6 x 10^{-5} M) during the next 3 hours. Pb concentration then decreased by 33% (6.4 x 10^{-5} M) over the next 7 days. The Pb evolution after the second leaching step exhibited the same pattern as previously. The modeled evolution of the pH in the leachate is represented with the measured values in Fig. 1.b, and an overall good fit with the data was observed (NRMSE = 7%), except for the first point at 7 days. A significant drop was recorded over the first 14 days from pH 6 to pH 4, before remaining constant around pH 4. The initial pH value in the simulations was 6, then a sharp drop of almost 2 pH units was observed during the first day, leading to a pH value of 4.15. The pH then rose slightly to the value of 4.2 during the remaining 6 days of the first leaching step. During the first day following the second leaching step a slight acidification was observed, the pH value reaching 4.1, then as before the pH increased up to the value of 4.2. As for the Pb evolution, the pH after the second leaching step exhibited a similar pattern than before.

The simulations showed that the main processes controlling the mobility of Pb were the dissolution and precipitation of the carrier phases. During the first leaching step the SI of the Pb-bearing phases (anglesite, plumbojarosite) decreased sharply, whereas they were initially close to zero and thus to equilibrium. This indicated an undersaturation of these minerals with respect to the new solution. Both these minerals dissolved, increasing the Pb concentrations in solution (Fig. 1.a). Anglesite quickly reached equilibrium (≈200 seconds) while plumbojarosite was always undersaturated and continued to dissolve (Fig. 2.a). Plumbojarosite also released Fe in solution which induced the precipitation of ferrihydrite (Fig. 2.b). This precipitation caused a drop in pH to 4.15, which led to the desorption of Pb from ferrihydrite. 80% of the initially sorbed Pb was released during the first days of the simulation, then the quantity of sorbed Pb remained constant until the end of the simulation. (Fig A.4a). Several studies have shown a link between the dissolution of jarosite and the precipitation of ferrihydrite (Welch et al., 2008; Elwood Madden et al., 2012). It has also been observed that this precipitation generated an acidification similar to our study, i.e. pH equal to

3.5 (Smith et al., 2006). Few hours after each watering step, anglesite became oversaturated and incorporated Pb by precipitating (Fig. 2.a); it has been reported that Pb resulting from the dissolution of plumbojarosite can be scavenged by the formation of anglesite (Lu and Wang, 2012). Pb in solution then decreased sharply, plumbojarosite being undersaturated, then decreased less as plumbojarosite approached equilibrium. In order to correctly predict the measured values, smaller surface areas were used for anglesite and plumbojarosite in the simulations than those measured on pure samples, namely 0.03 $m^2\ g^{-1}$ instead of 0.9 $m^2\ g^{-1}$ for anglesite (Zhang and Ryan, 1998) and 0.07 $m^2\ g^{-1}$ instead of 2.3 $m^2\ g^{-1}$ for plumbojarosite (Asta et al., 2009). This can be explained by the soil aggregation phenomenon and the presence of iron oxide coating, only part of the minerals then being accessible in the soil. Likewise, to obtain a good prediction of Pb concentration, the kinetic constants used for anglesite were reduced and they approached the values measured for barite $BaSO_4$ according to Dove and Czank (1995). The slight increase in pH during the last 6 days of the leaching step was caused by the dissolution of anorthite that consumed H^+, and also released Ca^{2+} (Fig. A.2).

During the second leaching step the processes were similar. Due to dilution with the leaching water anglesite and plumbojarosite dissolved, leading to a significant increase in Pb in solution (up to 9.5 x 10^{-5} M). Anglesite became oversaturated and precipitated which decreased the Pb concentration in solution. The dissolution of plumbojarosite at each step helped to maintain an acidic medium (pH=4.2) throughout the experiment. Pb and pH evolutions after the second leaching step were then comparable to that after the first, the mechanisms being identical. The results of the uncertainty analysis performed with PEST indicate a good robustness of the model (Table 2). Pb, Zn, pH and $SO^4{}_2^-$ were correctly described in the range of values considered, resulting in confidence limits close to the initial value. Anglesite and plumbojarosite were barely kinetically constrained and quickly reached thermodynamic equilibrium. Their behaviour was then mostly independent of their surface area.

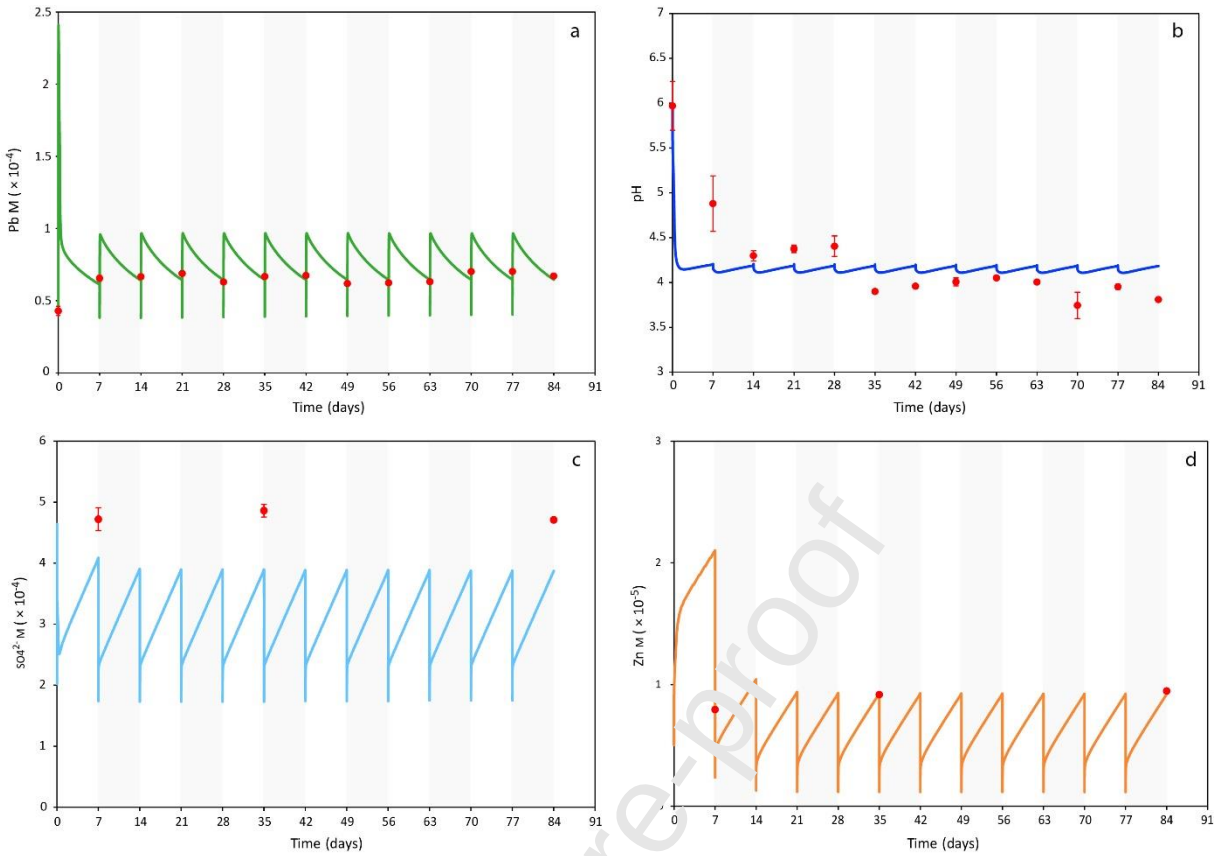

Fig. 1. Evolution with time of (a) Pb concentration, (b) pH, (c) SO_4^{2-} concentration, and (d) Zn concentration in solution, in the case of leaching experiments with tailings without amendments. Red dots correspond to experimental data (Thouin et al., 2019), and solid lines to calculated values.

The simulated evolution of SO_4^{2-} concentration in the leachate is compared to the measured values in Fig. 1.c. The predicted values of the model were in line with the measured values (NRMSE = 15.7%). The values of SO_4^{2-} concentration measured in the leachate remained constant at 4.6 x 10^{-4} M. In our simulation a similar pattern was observed for each leaching step. Immediately after watering, SO_4^{2-} concentration dropped from 3.9 x 10^{-4} M to 1.75 x 10^{-4} M, i.e. a decrease of 55%. Then SO_4^{2-} concentration increased quickly to 2.3 x 10^{-4} M within an hour. Finally, the increase continued at a slower rate, resulting in a 70% increase at the end of the leaching step. The dynamics of SO_4^{2-} was controlled by both plumbojarosite and anglesite. The quantity of SO_4^{2-} released from the dissolution of plumbojarosite was greater than the quantity of SO_4^{2-} incorporated due to anglesite precipitation. Thus, the SO_4^{2-} concentration in solution tended to increase. The decrease in

SO_4^{2-} concentration immediately after watering was due to dilution with mineral water (Mont Roucous). As a result, plumbojarosite dissolved rapidly because of its undersaturation. SO_4^{2-} concentration then continued to increase because plumbojarosite approached thermodynamic equilibrium without ever reaching it.

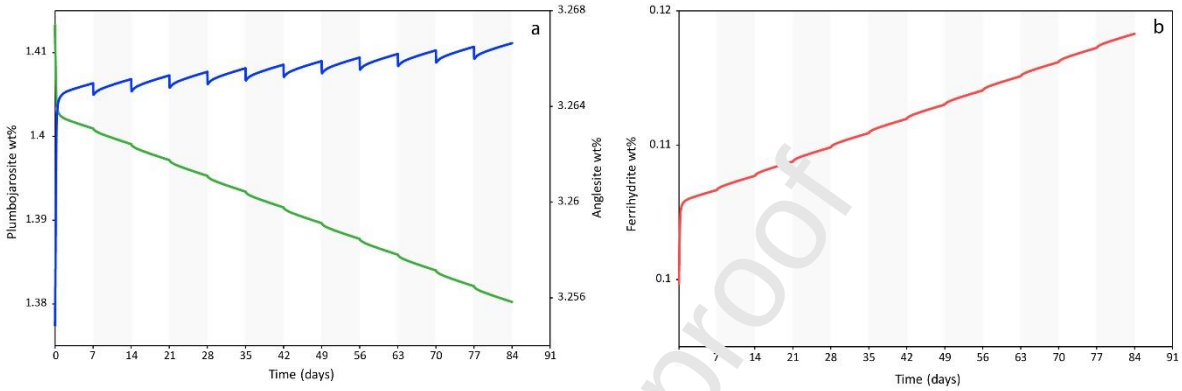

Fig. 2. Modelling of mineral dynamics during the leaching experiment of tailings without amendment (T): (a) content of anglesite (solid blue line) and plumbojarosite (solid green line), (b) content of ferrihydrite (solid red line).

The simulated evolution of Zn concentration in the leachate is represented with the measured values in Fig. 1.d. The NRMSE calculated value (85%) did not reflect well the effectiveness of the prediction due to the very low number of measured data (3), the first observation point drastically increasing the residual error (NRMSE = 2.6% without the first point). Zn concentration values measured in the leachate remained constant at 8.5 x 10^{-5} M. During the first day of the simulation, Zn concentration increased rapidly up to 1.6 x 10^{-5} M, i.e. an increase of 100%. The increase continued at a slower rate during the remaining 6 days of the first leaching step, reaching the value of 2.1 x 10^{-5} M. Immediately after watering, Zn concentration dropped to a value ten times lower (2.4 x 10^{-6} M), before rising up to 4.4 x 10^{-6} M after an hour. Then the increase continued more slowly, and at the end of the second leaching step the Zn concentration had increased by 125% (1 x 10^{-5} M). Zn evolution was similar for the following leaching steps. To explain the evolution of Zn in solution (Fig. 1.d), 0.5wt% of Zn was incorporated into plumbojarosite and 0.4wt% in anglesite. After the first

leaching step plumbojarosite was strongly undersaturated, which led to a significant dissolution of this mineral and thereby a significant increase of Zn in solution (up to 2.1 x 10^{-5} M) (Fig. 2.a). At the same time, anglesite precipitated, incorporating Zn into its structure. Due to the higher Zn proportion in plumbojarosite, Zn concentration in solution tended to increase. This increase slowed down after the first day because plumbojarosite was close to equilibrium. After the following leaching step Zn concentration strongly decreased thanks to the dilution effect before increasing again via plumbojarosite dissolution. Due to the low pH of the solution, a small amount of Zn was adsorbed on iron oxides (Fig A.4b). The dynamics of Zn in solution was then mainly controlled by the dissolution of Zn bearing phases.

3.2 Tailings amended with ochre (TO)

When the modeled evolution of Pb concentration in the leachate was compared to measured values (Fig. 3.a), the predictions were found to correctly match the data (NRMSE = 50.4%). The measurements carried out in the leachate revealed that Pb concentration remained constant at around 5 x 10^{-7} M, which represents a significant drop of 2 orders of magnitude compared to Pb concentrations measured in the leachate of the tailings alone (around 6.5 x 10^{-5} M). The model reproduced this drop well, the value at the start of the simulation being 2 x 10^{-7} M. Pb concentration increased by 8% during the first 36 hours, then more slowly at a constant rate of about 5% every 7 days. Concerning pH, the model matched the data very well (NRMSE = 6.4%) (Fig. 3.b). The pH measured in the leachate was 6.7 before increasing to 7.7 and then remained constant. This represented a sharp increase in pH compared to the tailing alone which had a pH of 4. The increase in pH was reproduced in the simulation: the pH value was 7.7 initially, and then remained constant until the end.

Pb concentration in the leachate after the addition of ochre was more than 100 times lower than for the tailing alone (Fig. 3.a). This decrease was mainly explained by the increase in pH induced by the dissolution of aragonite brought by ochre. Although aragonite

and calcite exhibit a similar behaviour and buffering pH range (Wahlström et al., 2009), aragonite is less common in tailings and therefore less studied, unlike calcite, whose buffering capacity in mine tailings is well known (Zhu et al., 2002; Gunsinger et al., 2006), stabilizing the pH at a neutral level. Consequently, more Pb can be adsorbed onto ferrihydrite due to the deprotonation of surface sites (Fig A.5a). In addition, the dissolution of plumbojarosite caused the precipitation of ferrihydrite, increasing the number of sites available for sorption (Fig. 4.c). During the 3 days of contact before the start of the experiment, the pH which was initially 6 increased to 7.7. This caused the dissolution of 85% of the aragonite present in ochre. The dissolution rate of aragonite then decreased because its SI was close to zero, limiting a pH increase. Similar values were observed in a tailing at neutral conditions due to the presence of calcite (Gunsinger et al., 2006). Aragonite also released Ca, and in greater quantities than anorthite (Fig A.3). Following the increase in pH, the dissolution rate of plumbojarosite increased sharply. 90% of the plumbojarosite was dissolved during the 3 days of contact before the start of the experiment, and almost all at the end of the first week (Fig. 4.a). Gunsinger et al. (2006) calculated the saturation index of plumbojarosite in pore water, and observed a stronger undersaturation at neutral pH than at acidic pH. This seems to confirm that plumbojarosite dissolved more strongly at neutral pH when sorption was significant and acted as a sink for Pb in solution. After 7 days, the evolution of Pb concentration was controlled by two phenomena: firstly, the renewal of the pore water caused Pb desorption from ferrihydrite, generating a baseline level around 2.4 x 10^{-7} M; secondly, anglesite continued to dissolve at a fairly slow rate, causing a slight increase in Pb over time. It was assumed that the large amount of iron oxide added by ochre coated the minerals, thus reducing the surface area by an order of magnitude for anglesite and plumbojarosite.

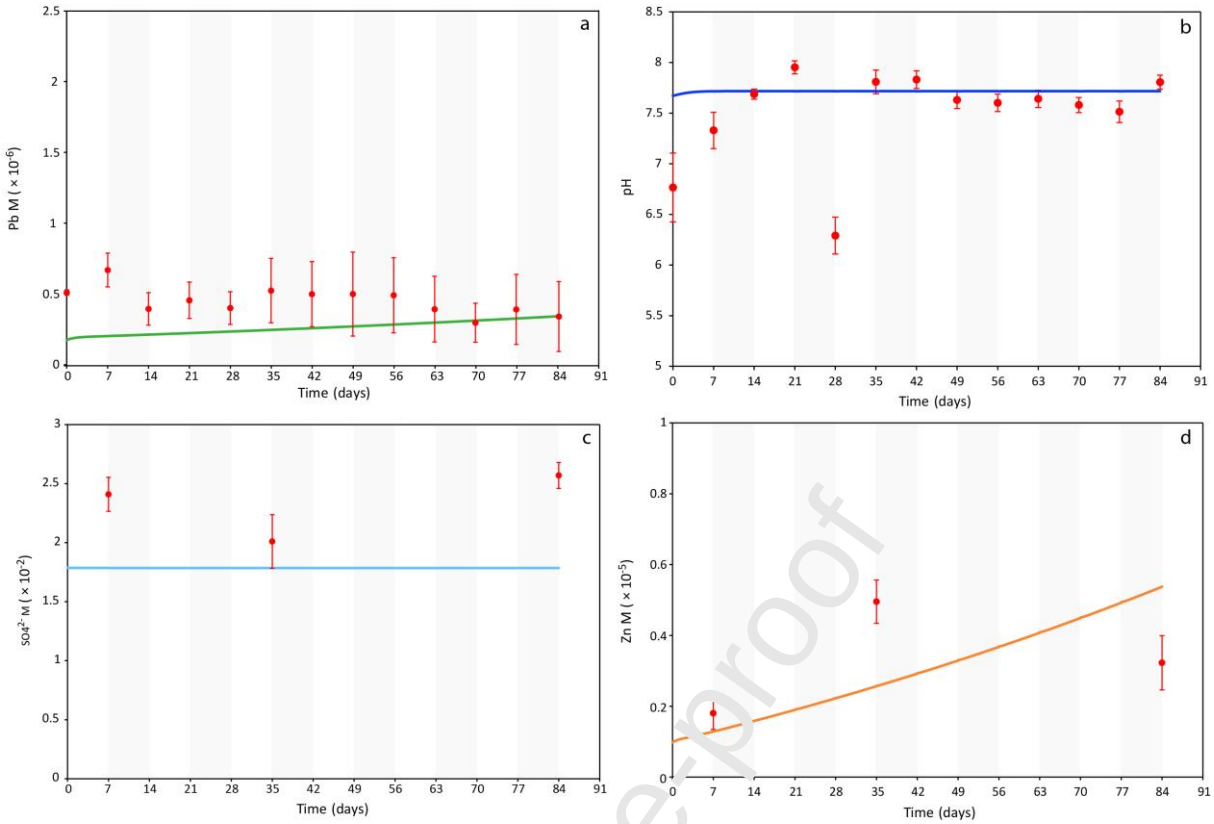

Fig. 3. Evolution with time of (a) Pb concentration, (b) pH, (c) SO_4^{2-} concentration, and (d) Zn concentration in solution, in the case of leaching experiments with tailings amended with 5wt% ochre (TO). Red dots correspond to experimental data (Thouin et al., 2019), and solid lines to calculated values.

Concerning the evolution of SO_4^{2-} concentration in the leachate, the simulation correctly predicted the measured data (NRMSE = 25%) (Fig. 3.c). Measured values remained constant during the experiment at around 2.3 x 10^{-2} M, while predicted values remained constant at 1.8 x 10^{-2} M. Under these conditions, the SO_4^{2-} release from Pb-bearing phases (anglesite and plumbojarosite) played a negligible role in the dynamics of SO_4^{2-}. Gypsum dissolution mainly constrained this concentration and depicted a reactive behavior (Fig. 4.b). This mineral exhibited a strong dissolution at each watering step, a thermodynamic equilibrium was quickly reached and the amount of gypsum remained constant until the next step.

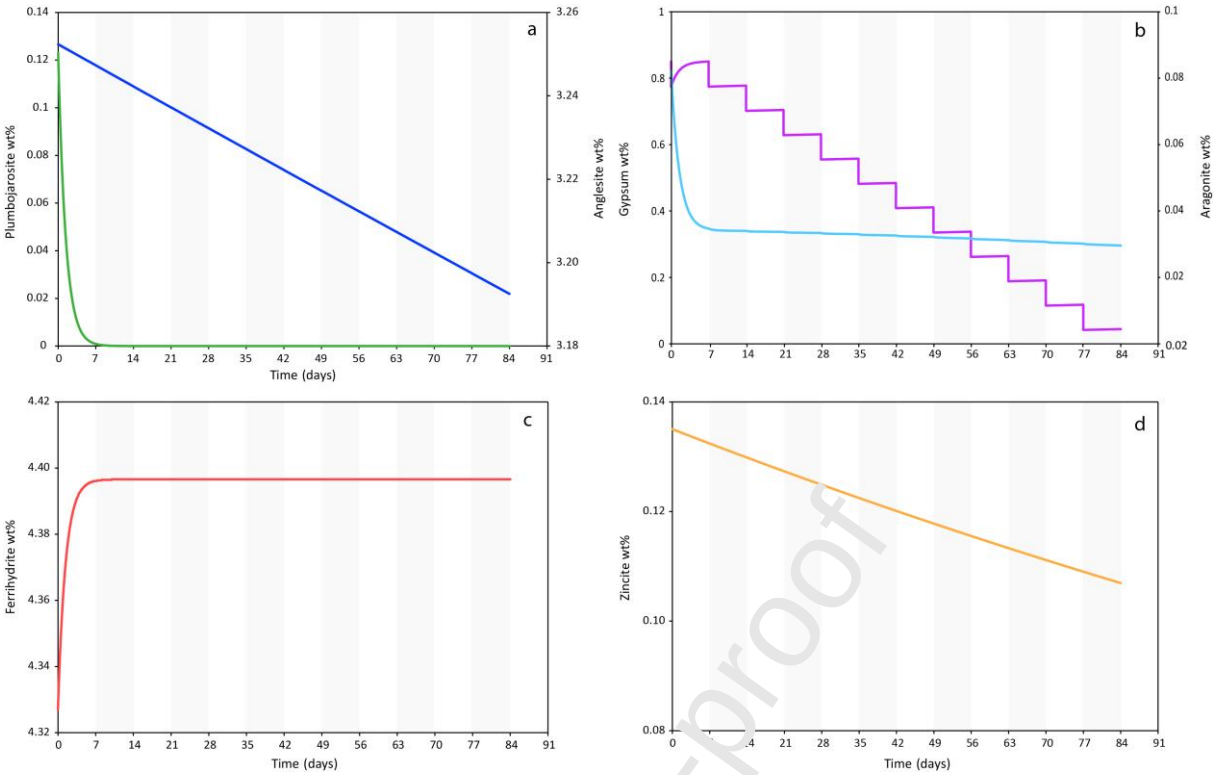

Fig. 4. Modelling of mineral dynamics during the leaching experiment for the tailings amended with ochre (TO): (a) content of plumbojarosite (solid green line) and anglesite (solid dark blue line), (b) content of aragonite (solid light blue line) and gypsum (solid purple line), (c) content of ferrihydrite (solid red line), (d) content of zincite (solid orange line).

For the simulated evolution of Zn concentration in the leachate compared to measured values, the calculated NRMSE value (56.2%) was quite high, but the relevance of this value is questionable in view of the small set of data (Fig. 3.d). The measured Zn concentration in the leachate remained constant around 3 x 10^{-6} M. The simulated Zn concentration, initially 1.1 x 10^{-6} M, increased throughout the experiment with an increase of about 4 x 10^{-7} M every week. This increase was mainly due to the dissolution of zincite and anglesite, as plumbojarosite had been almost completely dissolved after 7 days (Fig. 4.a and 4.d). The adsorption capacity of ferrihydrite formed a sink for Zn (Fig A.5b), preventing zincite from reaching thermodynamic equilibrium.

3.3 Tailings amended with ochre and manure (TOM)

The simulated and measured Pb concentrations in the leachate for the three proportions of manure are shown in Fig. 5.a. The model was able to reproduce the data quite faithfully for Pb (NRMSE = 48.4%, 41.4%, and 37%, for 0.15wt%, 1wt% and 2wt% manure, respectively). The measured Pb concentrations revealed a different evolution depending on the proportion of manure added. With 0.15%, the concentration remained stable at around 2.5 x 10^{-7} M, i.e. a similar evolution to that of TO. With 1 and 2wt% of manure, the Pb concentration increased to 1.5 x 10^{-6} M after 35 days before decreasing to a value close to the initial one after 84 days.

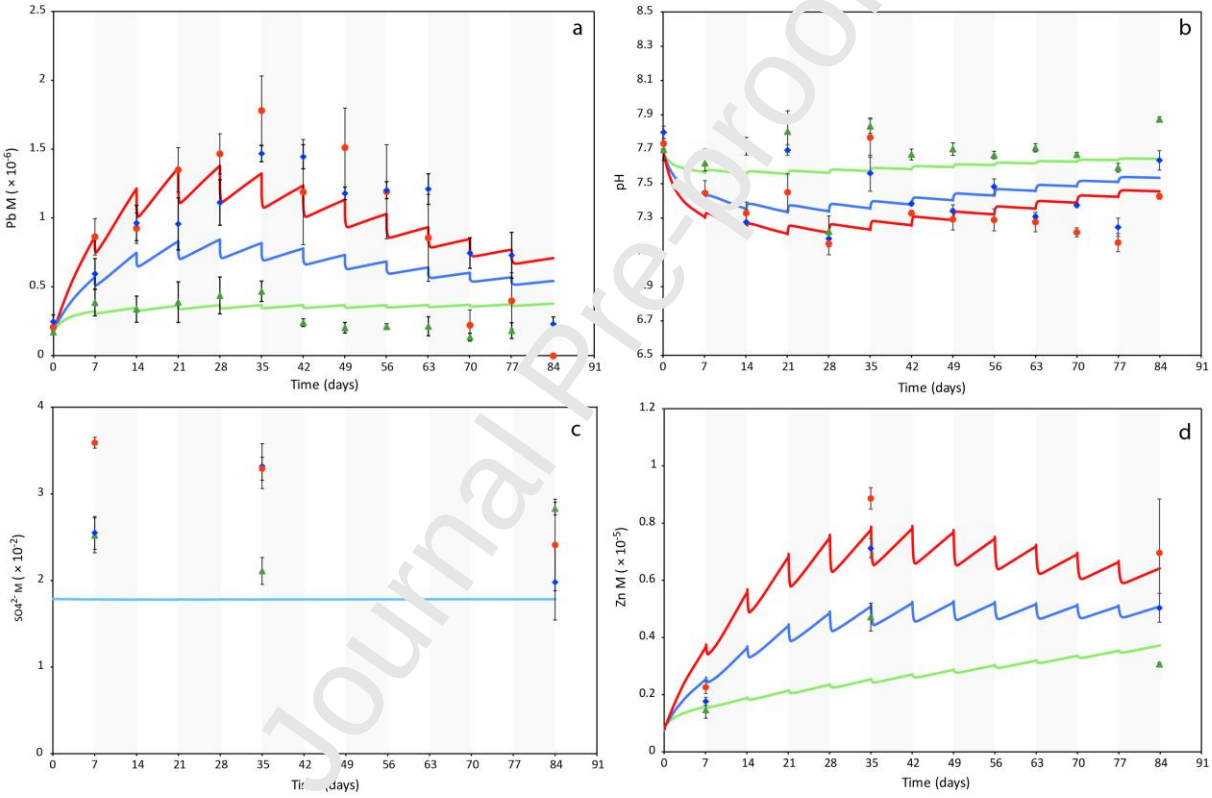

Fig. 5. Evolution with time of (a) Pb concentration, (b) pH, (c) SO_4^{2-} concentration, and (d) Zn concentration in solution, in the case of leaching experiments with tailings amended with 5wt% ochre and manure with variable proportions (TOM). Red dots correspond to experimental data (Thouin et al., 2019), and solid lines to calculated values. The red line corresponds to 2wt% manure, the blue line to 1wt% manure, and the green line to 0.15wt% manure. The light blue solid line represents the three proportions, the evolution of SO_4^{2-} concentration being independent of the amount of manure.

The simulated evolution of Pb presented several patterns at different time scales. The first pattern extended over a period of 7 days and corresponded to a continuous increase in Pb concentration before a sudden drop. For all manure proportions, the increase during the first 7 days was the largest, corresponding to an increase of 95%, 245% and 420% for 0.15, 1 and 2wt% respectively. This phenomenon then slowed down during the last week with an increase of 4%, 5% and 6% for 0.15, 1 and 2wt% respectively. The decrease in Pb concentration occurred immediately after watering. The higher the amount of manure, the more significant the drop was, with variations ranging from 3 to 6%, 10 to 15% and 13 to 18% for 0.15, 1 and 2wt% respectively. The second pattern extended over the entire duration of the experiment and was only significant for 1 and 2wt%. It corresponded to an increase in Pb concentration during approximately the first half of the experiment (28 days) then a decrease during the remaining time of the experiment. Pb concentration changed from 1.9 x 10^{-7} M to 8.4 x 10^{-7} M for 1wt% and from 1.9 x 10^{-7} M to 1.4 x 10^{-6} M for 2wt% during the first 28 days. The decrease in concentration was less pronounced, with Pb concentration at 84 days reaching 5.4 x 10^{-7} M for 1 wt% and 7.1 x 10^{-7} M for 2wt%. The second pattern was quite different for the TOM 0.15 condition. No decrease in concentration was observed; a significant increase took place during the first 28 days then the Pb concentration remained globally constant at a value of 3.7 x 10^{-7} M until the end of the experiment. Concerning pH, the model correctly fitted the data: NRMSE = 2.2%, 2.3% and 2.7% for 0.15, 1 and 2wt% manure, respectively (Fig. 5.b). As for Pb concentration, the measured pH values varied according to the proportion of manure. With 0.15wt%, pH remained constant around 7.7. For 1 and 2wt% acidification took place during the first 35 days resulting in a pH of 7.2, then a slight rise in pH was observed during the rest of the experiment reaching a pH of 7.5-7.6. The evolution of the simulated pH followed two patterns similar to those of Pb but in the opposite direction. The first pattern extended over a period of 7 days and corresponded to a continuous decrease in the pH values before a sudden rise. The drop in pH value was greater during the first 7 days with a decrease of 0.15, 0.3 and 0.4 pH units for 0.15, 1 and

2wt% respectively. This trend slowed down over time, the decrease in pH value observed during the last leaching step being almost zero. Immediately after watering, the pH value sharply increased for all the leaching steps. As for Pb, the greater the quantity of manure was, the greater the changes were. The second pattern extended over the three months of the experiment, and corresponded to the pH decrease during approximately the first half of the experiment (28 days) for TOM 1 (from 7.7 to 7.33) and TOM 2 (from 7.7 to 7.22) and only significantly during the first 7 days for TOM 0.15. This decrease was followed by an increase during the remaining time of the experiment, but reaching final pH values lower than the initial ones (7.53 for 1wt% and 7.45 for 2wt%). For 0.15wt% the decrease of pH only occurred during the first week, the pH decreasing from 7.7 to 7.55. The pH rise phase therefore took place over a longer period, reaching a final pH value of 7.64 close to the initial one.

The variation in Pb concentration according to the quantity of manure added cannot be explained by the dissolution of the bearing phases since the dynamic of Pb bearing mineral phases was independent of the amount of manure (Fig.6.c). Simulations showed that the different Pb concentrations depending on the amount of manure were controlled by pH. With low added manure (0.15wt%) the measured pH values were similar to those of TO, i.e. 7.7 (Fig. 5.a). With the addition of 1 and 2wt% manure, a slight acidification was recorded (up to 7.2). This acidification was attributed to microbial respiration, enhanced by the addition of organic matter, which released CO_2 in solution. The link between microbial activity in soil and CO_2 production is well known in the literature (Stotzky, 1965). Moreover, numerous studies have highlighted that the addition of organic amendments increases the production of CO_2 (Neilson and Pepper, 1990; Li et al., 2013). Then, a larger amount of manure allowed the increase of microbial respiration, leading to an oversaturation of CO_2 in solution (Fig. 6.b). During the first leaching step the concentration of dissolved CO_2 increased rapidly due to the high amount of organic carbon available (Fig. 6.a). At each leaching step the CO_2 concentration instantly decreased due to the mix between the soil gases and the

atmosphere. The acidification induced by microbial respiration prevented the sorption of Pb on iron oxides and organic matter, although the sorption of Pb was greater on iron oxides than on organic matter (Fig A.6a and Fig A6b). The amount of soluble organic matter decreased exponentially, limiting microbial respiration and the release of CO_2. Thus, due to the successive mixtures between soil gases and atmosphere, the concentration of dissolved CO_2 decreased, resulting in the rise of pH. The decrease of the proton concentration allowed a greater sorption of Pb. The reactivity of the Pb-bearing phases remained unchanged. Plumbojarosite was completely dissolved and the dissolution of anglesite was mainly controlled by Pb concentration in solution and kinetically limited. This dynamic was illustrated in Fig. 6.c where the evolution of the Pb-bearing phases was independent of the quantity of manure added and therefore of the intensity of the acidification. The results of the uncertainty analysis carried out with PEST for TO and TOM 1% simulation showed a higher uncertainty than for the simulation of the tailings only (Table 2). The estimated PEST value was similar to the initial value for anglesite but was 28% higher for plumbojarosite. The confidence limits were ± 18% for anglesite and ± 8% for plumbojarosite. These results suggest a greater kinetic control after the addition of amendments, kinetic parameters like the surface area were then more important in the reactivity of the system. However, there are still large gaps in determining precisely these parameters, coating effects may take place when adding amendments.

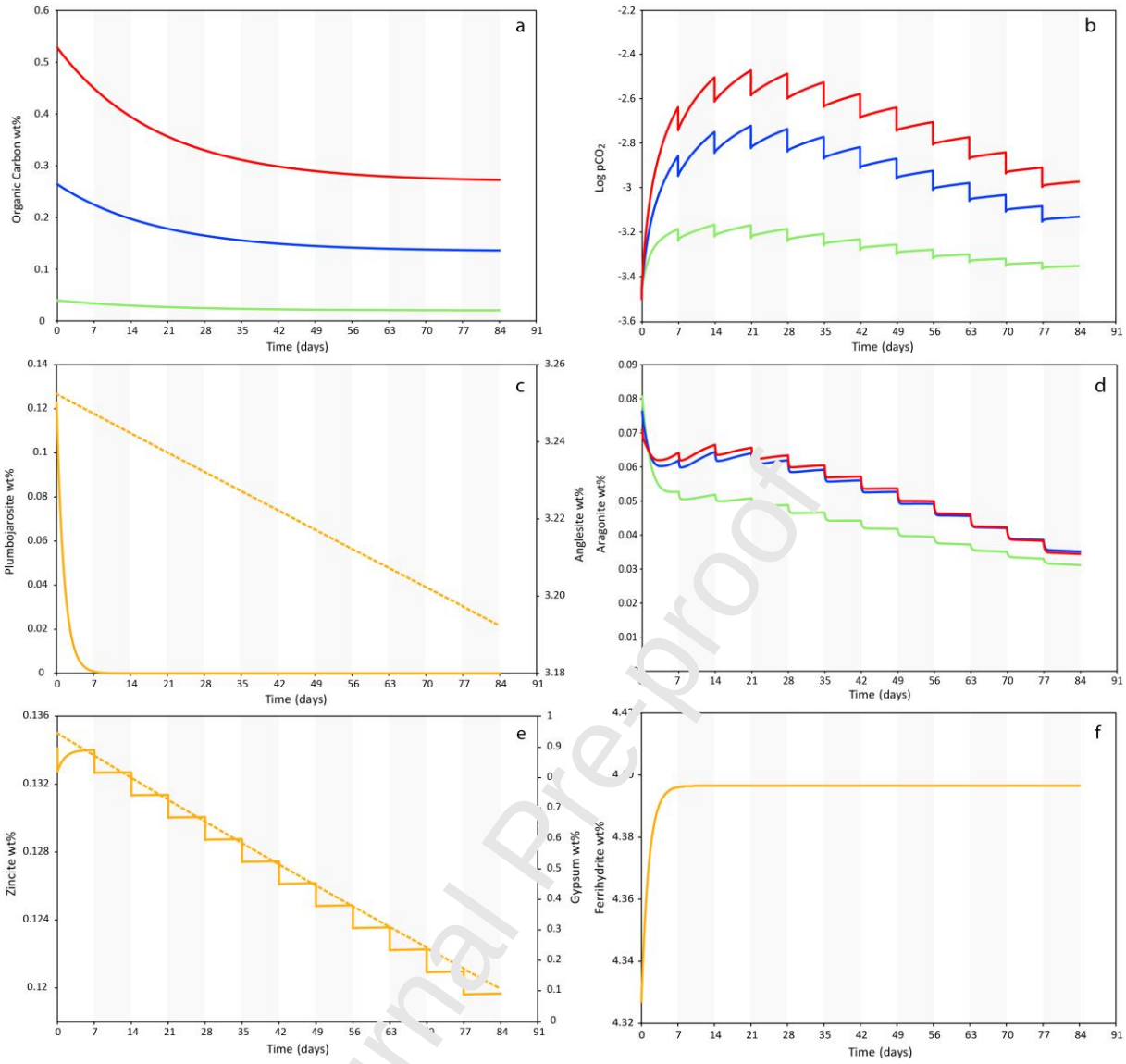

Fig. 6. Modelling of mineral dynamics during the leaching experiment for the tailings amended with ochre and manure (TOM). Red lines correspond to 2wt% manure, blue lines to 1wt% manure, green lines to 0.15wt% manure and orange lines to a mean evolution of the three proportions: (a) content of solubilizable organic carbon, (b) Log pCO_2, (c) content of plumbojarosite (solid line) and anglesite (dashed line), (d) content of aragonite, (e) content of zincite (dashed line) and gypsum (solid line), (f) content of ferrihydrite.

The evolution of measured and simulated SO_4^{2-} concentration was similar to that observed for the TO treatment (Fig. 5.c). The model reproduced the data quite faithfully (NRMSE = 30%, 37% and 45%, for 0.15, 1 and 2wt% manure, respectively). The measured

SO_4^{2-} concentrations remained globally constant during the leaching experiment for the three proportions of manure, with a variation in the concentrations between 2 x 10^{-2} M and 3.5 x 10^{-2} M. The dynamics of simulated SO_4^{2-} were mainly controlled by gypsum (Fig. 6.e), so manure did not affect SO_4^{2-} concentration in solution.

The predictions of Zn concentration in the leachate produced by the model correctly matched the data, with NRMSE = 42.5%, 27.1% and 34.5% for 0.15, 1 and 2wt% manure, respectively (Fig. 5.d). As for Pb concentration, the measured Zn concentration showed an increase during the first half of the experiment (of 220%, 300% and 290% for 0.15, 1 and 2wt% manure, respectively), then a decrease (of 35%, 29% and 21% for 0.15, 1 and 2wt% manure, respectively). The dynamics of simulated Zn were quite similar to that of Pb. For each proportion of manure, Zn concentration followed a pattern which extended over a period of 7 days, with a continuous increase before a sharp drop between each leaching step. The second pattern, which consisted of an increase and then a decrease in concentration over time, was less predominant for Zn than for Pb. Zn concentration increased during the first 42 days, from 1 x 10^{-6} M to 5.2 x 10^{-6} M for 1wt% manure and from 1 x 10^{-6} M to 7.8 x 10^{-6} M for 2wt%. Between 42 and 84 days Zn concentration decreased by 18% for 2wt% manure and while it remained constant for 1wt%. For 0.15wt% manure it increased slightly and continuously, with an increase of approximately 5% between each leaching step. The evolution of Zn can be explained in the same way as for Pb. The first pattern is explained by the renewal of pore water and the mix with the atmosphere, which increased pH and decreased the concentration in solution. The second pattern is explained by the acidification caused by microbial respiration. Then, this microbial activity slowed down due to the decrease in available organic matter. The drop in Zn concentration was less pronounced than for Pb concentration because zincite continued to dissolve (Fig. 6.e), releasing Zn in solution. This also explains the slight increase in Zn observed for TOM 0.15. As for Pb, Zn adsorbed much more on ferrihydrite than on organic matter (Fig. A.6c and Fig. A.6d). A summary of highlighted processes for the different simulations is illustrated in Fig. 7.

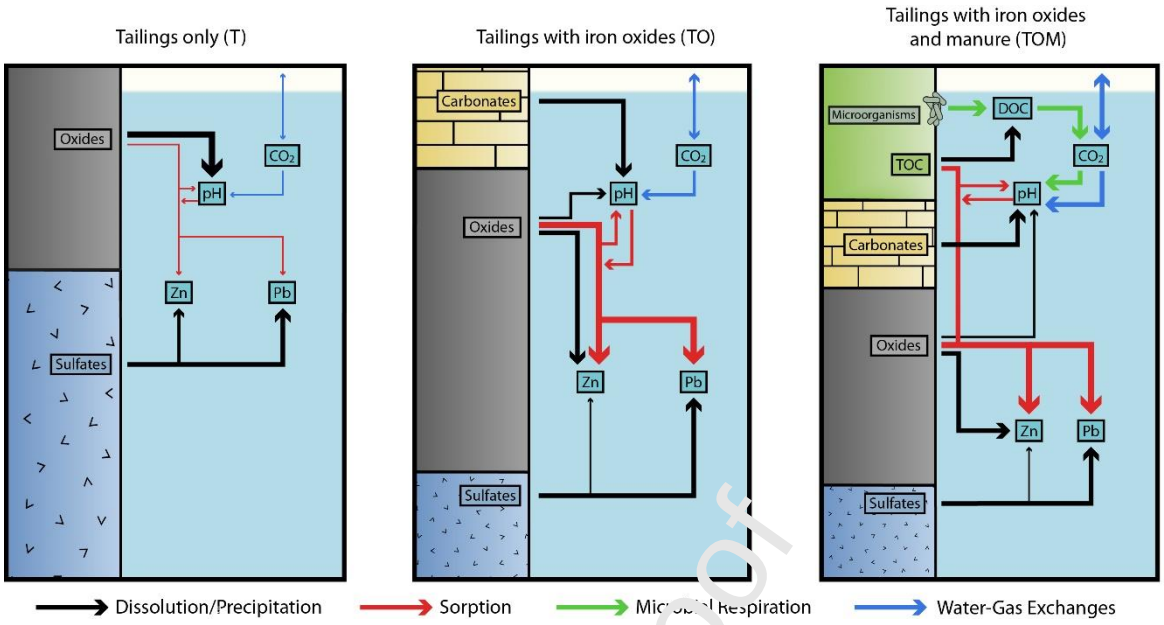

Fig. 7. Impact of geochemical processes on the modeled parameters (pH, Pb, Zn) for the different simulations (T, TO and TOM). Processes are indicated by colored arrows, while the magnitude of the processes is depicted by the thickness of the arrows.

4. Conclusion

Leaching data were used to develop a geochemical model that combines the key processes involved in mining soils: adsorption, water-gas exchanges, microbial respiration, dissolution and precipitation. In the case of tailings without amendments, the dissolution of secondary phases such as anglesite and plumbojarosite was the main process controlling metal concentrations (Pb, Zn) in solution. The release of Fe induced by the dissolution of plumbojarosite allowed the precipitation of ferrihydrite which maintained the pH at an acid level (≈4). Surface reactions have a low impact in the overall dynamics due to the acidic conditions. The pH rose significantly (pH = 7.7) by applying mining slurry consisting of Fe oxide-hydroxide combined with minor aragonite to the tailings. A greater quantity of Pb and Zn was sorbed onto Fe oxides due to the reduced competition with protons and the greater number of available sorption sites. This contributed to accelerating the dissolution of Pb and

Zn bearing phases. Therefore the sorption and desorption mechanisms became the major controls on the metal concentrations in solution. Finally, the addition of organic matter through manure amplified the microbial activity and consequently the production of CO_2. This led to a slight pore-water acidification (from 7.7 to 7.2) and then a release of metals by limiting their sorption on organic matter and Fe oxides. The quantity of soluble organic matter then decreased, limiting microbial respiration and the release of CO_2. This study has provided key information on the nature and extent of the biogeochemical processes that control the mobility of metals in aged tailings. This modelling approach can be a valuable decision-making tool in order to provide an optimal management plan for these aged mining sites. In further studies, this geochemical model could be coupled with a detailed water flow model in order to describe precisely the pathway of metal contaminants in this system.

Acknowledgements

This research was performed within the framework of the Phytoselect project funded by the Région Centre - Val de Loire (contract N°2016-00108485), and by the Labex Voltaire (ANR-10-LABX-100-01). S. Mertz benefits from a Ph.D. grant provided by the French geological survey (BRGM) and by the Région Centre – Val de Loire. The authors would like to acknowledge the three reviewers for their helpful comments and suggestions. Finally, the authors thank Elizabeth Rowley-Jolivet for English editing.

References

Acero, P., Ayora, C., Carrera, J., Saaltink, M.W., Olivella, S., 2009. Multiphase flow and reactive transport model in vadose tailings. Appl. Geochem. 24, 1238–1250. https://doi.org/10.1016/j.apgeochem.2009.03.008

Acosta, J.A., Abbaspour, A., Martínez, G.R., Martínez-Martínez, S., Zornoza, R., Gabarrón, M., Faz, A., 2018. Phytoremediation of mine tailings with Atriplex halimus and organic/inorganic amendments: A five-year field case study. Chemosphere 204, 71–78. https://doi.org/10.1016/j.chemosphere.2018.04.027

Akcil, A., Koldas, S., 2006. Acid Mine Drainage (AMD): causes, treatment and case studies. J. Clean. Prod. 14, 1139–1145. https://doi.org/10.1016/j.jclepro.2004.09.006

Al-Abed, S., Jegadeesan, G., Purandare, J., Allen, D., 2008. Leaching behavior of mineral processing waste: Comparison of batch and column investigations. J. Hazard. Mater. 153, 1088–1092. https://doi.org/10.1016/j.jhazmat.2007.09.063

Appelo, C.A.J., Postma, D., 2005. Geochemistry, groundwater and pollution, 2. ed., 10., corr. repr. ed. CRC Press [u.a.], Boca Raton.

Asta, M.P., Cama, J., Martínez, M., Giménez, J., 2009. Arsenic removal by goethite and jarosite in acidic conditions and its environmental implications. J. Hazard. Mater. 171, 965–972. https://doi.org/10.1016/j.jhazmat.2009.06.097

Atanacković, N., Dragišić, V., Stojković, J., Papić, P., Živanović, V., 2013. Hydrochemical characteristics of mine waters from abandoned mining sites in Serbia and their impact on surface water quality. Environ. Sci. Pollut. Res. 20, 7615–7626. https://doi.org/10.1007/s11356-013-1959-4

Blanc, Ph., Lassin, A., Piantone, P., Azaroual, M., Jacquemet, N., Fabbri, A., Gaucher, E.C., 2012. Thermoddem: A geochemical database focused on low temperature water/rock interactions and waste materials. Appl. Geochem. 27, 2107–2116. https://doi.org/10.1016/j.apgeochem.2012.06.002

Blowes, D.W., Jambor, J.L., 1990. The pore-water geochemistry and the mineralogy of the vadose zone of sulfide tailings, Waite Amulet, Quebec, Canada. Appl. Geochem. 5, 327–346. https://doi.org/10.1016/0883-2927(90)90008-S

Bori, J., Vallès, B., Navarro, A., Riva, M.C., 2016. Geochemistry and environmental threats of soils surrounding an abandoned mercury mine. Environ. Sci. Pollut. Res. 23, 12941–12953. https://doi.org/10.1007/s11356-016-6463-1

BRGM, 1997. Les résidus miniers français: typologie et principaux impacts environnementaux potentiels (No. R 39503).

Bril, H., Zainoun, K., Puziewicz, J., Courtin-Nomade, A., Vanaecker, M., Bollinger, J.-C., 2008. Secondary phases from the alteration of a pile of zinc-smelting slag as indicators of environmental conditions: an example from Swietochlowize, upper Silesia, Poland. Can. Mineral. 46, 1235-1248. https://doi.org/10.3749/canmin.46.5.1235

Cappuyns, V., Alian, V., Vassilieva, E., Swennen, R., 2014. pH Dependent Leaching Behavior of Zn, Cd, Pb, Cu and As from Mining Wastes and Slags: Kinetics and Mineralogical Control. Waste Biomass Valori. 5, 355–368. https://doi.org/10.1007/s12649-013-9274-3

Courtin-Nomade, A., Waltzing, T., Evrard, C., Soubrand, M., Lenain, J.-F., Ducloux, E., Ghorbel, S., Grosbois, C., Bril, H., 2016. Arsenic and lead mobility: From tailing materials to the aqueous compartment. Appl. Geochem. 64, 10–21. https://doi.org/10.1016/j.apgeochem.2015.11.002

Davis Jr., R.A., Welty, A.T., Borrego, J., Morales, J.A., Pendon, J.G., Ryan, J.G., 2000. Rio Tinto estuary (Spain): 5000 years of pollution. Environ. Geol. 39, 1107–1116. https://doi.org/10.1007/s002549900096

Dean, J.A., 1999. Lange's Handbook of Chemistry, 15th ed. New York: McGraw-Hill.

Doherty, J., 2015. Calibration and uncertainty analysis for complex environmental models. Brisbane, Australia: Watermark Numerical Computing.

Dove, P.M., Czank, C.A., 1995. Crystal chemical controls on the dissolution kinetics of the isostructural sulfates: Celestite, anglesite, and barite. Geochim. Cosmochim. Acta 59, 1907–1915. https://doi.org/10.1016/0016-7037(95)00116-6

Dutrizac, J.E., 1984. The Behavior of Impurities during Jarosite Precipitation, in: Bautista, R.G. (Ed.), Hydrometallurgical Process Fundamentals. Springer US, Boston, MA, 125–169. https://doi.org/10.1007/978-1-4899-2274-8_6

Dzombak, D.A., Morel, F.M.M., 1990. Surface complexation modeling: hydrous ferric oxide. Wiley, New York.

Elwood Madden, M.E., Madden, A.S., Rimstidt, J.D., Zahrai, S., Kendall, M.R., Miller, M.A., 2012. Jarosite dissolution rates and nanoscale mineralogy. Geochim. Cosmochim. Acta 91, 306–321. https://doi.org/10.1016/j.gca.2012.05.001

Eriksson, N., Destouni, G., 1997. Combined effects of dissolution kinetics, secondary mineral precipitation, and preferential flow on copper leaching from mining waste rock. Water Resour. Res. 33, 471–483. https://doi.org/10.1029/96WR03466

Fellet, G., Marmiroli, M., Marchiol, L., 2014. Elements uptake by metal accumulator species grown on mine tailings amended with three types of biochar. Sci. Total Environ. 468–469, 598–608. https://doi.org/10.1016/j.scitotenv.2013.08.072

Francis, A.J., 1990. Microbial dissolution and stabilization of toxic metals and radionuclides in mixed wastes. Experientia 46, 840–851. https://doi.org/10.1007/BF01935535

Gemici, Ü., 2008. Evaluation of the water quality related to the acid mine drainage of an abandoned mercury mine (Alaşehir, Turkey). Environ. Monit. Assess. 147, 93–106. https://doi.org/10.1007/s10661-007-0101-9

Gerke, H.H., Molson, J.W., Frind, E.O., 1998. Modelling the effect of chemical heterogeneity on acidification and solute leaching in overburden mine spoils. J. Hydrol. 209, 166–185. https://doi.org/10.1016/S0022-1694(98)00106-1

Gerke, H.H., Molson, J.W., Frind, E.O., 2001. Modelling the impact of physical and chemical heterogeneity on solute leaching in pyritic overburden mine spoils. Ecol. Eng. 17, 91–101. https://doi.org/10.1016/S0925-8574(00)00150-6

Gunsinger, M.R., Ptacek, C.J., Blowes, D.W., Jambor, J.L., Moncur, M.C., 2006. Mechanisms controlling acid neutralization and metal mobility within a Ni-rich tailings impoundment. Appl. Geochem. 21, 1301–1321. https://doi.org/10.1016/j.apgeochem.2006.06.006

Harwood, J.J., Koirtyohann, S.R., 1987. Modelling of leachates from dolomitic mine tailings. Environ. Geochem. Health 9, 17–22. https://doi.org/10.1007/BF01811112

Jin, Q., Bethke, C.M., 2002. Kinetics of Electron Transfer through the Respiratory Chain. Biophys. J. 83, 1797–1808. https://doi.org/10.1016/S0006-3495(02)73945-3

Jin, Q., Bethke, C.M., 2003. A New Rate Law Describing Microbial Respiration. Applied and Environ. Microbiol. 69, 2340–2348. https://doi.org/10.1128/AEM.69.4.2340-2348.2003

Jing, C., Meng, X., Korfiatis, G., 2004. Lead leachability in stabilized/solidified soil samples evaluated with different leaching tests. J. Hazard. Mater. 114, 101–110. https://doi.org/10.1016/j.jhazmat.2004.07.017

Jurjovec, J., Ptacek, C.J., Blowes, D.W., 2002. Acid neutralization mechanisms and metal release in mine tailings: a laboratory column experiment. Geochim. Cosmochim. Acta 66, 1511–1523. https://doi.org/10.1016/S0016-7037(01)00874-2

Kashefi, K., Tor, J.M., Nevin, K.P., Lovley, D.R., 2001. Reductive Precipitation of Gold by Dissimilatory Fe(III)-Reducing Bacteria and Archaea. Appl. Environ. Microbiol. 67, 3275–3279. https://doi.org/10.1128/AEM.67.7.3275-3279.2001

Kelley, B.C., Tuovinen, O.H., 1988. Microbiological Oxidations of Minerals in Mine Tailings, in: Salomons, W., Förstner, U. (Eds.), Chemistry and Biology of Solid Waste. Springer Berlin Heidelberg, Berlin, Heidelberg, 33–53. https://doi.org/10.1007/978-3-642-72924-9_2

Kumpiene, J., Lagerkvist, A., Maurice, C., 2008. Stabilization of As, Cr, Cu, Pb and Zn in soil using amendments – A review. Waste Manage. 28, 215–225. https://doi.org/10.1016/j.wasman.2006.12.012

Lasaga, A.C., 1981. Transition state theory. Rev. Mineral. Geochem. 8, 135–168.

Lasaga, A.C., 1984. Chemical kinetics of water-rock interactions. J. Geophys. Res. 89, 4009–4025. https://doi.org/10.1029/JB089iB06p04009

Lebrun, M., Nandillon, R., Miard, F., Le Forestier, L., Morabito, D., Bourgerie, S., 2020. Effects of biochar, ochre and manure amendments associated to a metallicolous ecotype of *Agrostis capillaris* on As and Pb stabilization of a former mine technosol. Envir. Geochem. Health 182, 149-156. https://doi.org/10.1007/s10653-020-00592-5

Lee, J.-S., Chon, H.-T., Kim, K.-W., 2005. Human risk assessment of As, Cd, Cu and Zn in the abandoned metal mine site. Environ. Geochem. Health 27, 185–191. https://doi.org/10.1007/s10653-005-0131-6

Li, L.-J., You, M.-Y., Shi, H.-A., Ding, X.-L., Qiao, Y.-F., Han, X.-Z., 2013. Soil CO2 emissions from a cultivated Mollisol: Effects of organic amendments, soil temperature, and moisture. Eur.J. Soil Biol. 55, 83–90. https://doi.org/10.1016/j.ejsobi.2012.12.009

Lu, X., Wang, H., 2012. Microbial Oxidation of Sulfide Tailings and the Environmental Consequences. Elements 8, 119–124. https://doi.org/10.2113/gselements.8.2.119

Mayer, K.U., Frind, E.O., Blowes, D.W., 2002. Multicomponent reactive transport modeling in variably saturated porous media using a generalized formulation for kinetically controlled reactions: Reactive transport modeling in variably saturated media. Water Resour. Res. 38, 13-1-13–21. https://doi.org/10.1029/2001WR000862

McCarty, D.K., Moore, J.N., Marcus, W.A., 1998. Mineralogy and trace element association in an acid mine drainage iron oxide precipitate; comparison of selective extractions. Appl. Geochem. 13, 165–176. https://doi.org/10.1016/S0883-2927(97)00067-X

McHale, A.P., McHale, S., 1994. Microbial biosorption of metals: Potential in the treatment of metal pollution. Biotechnol. Adv. 12, 647–652. https://doi.org/10.1016/0734-9750(94)90005-1

Nandillon, R., Miard, F., Lebrun, M., Gaillard, M., Sabatier, S., Bourgerie, S., Battaglia-Brunet, F., Morabito, D., 2019. Effect of Biochar and Amendments on Pb and As Phytotoxicity and Phytoavailability in a Technosol. Clean - Soil, Air, Water 47, 1800220. https://doi.org/10.1002/clen.201800220

Neilson, J.W., Pepper, I.L., 1990. Soil Respiration as an Index of Soil Aeration. Soil Sci. Soc. Am. J. 54, 428–432. https://doi.org/10.2136/sssaj1990.03615995005400020022x

Norini, M.P., Thouin, H., Miard, F., Battaglia-Brunet, F., Gautret, P., Guégan, R., Le Forestier, L., Morabito, D., Bourgerie, S., Motelica-Heino, M., 2019. The ecodynamic of Pb, Zn, Ba, As and Cd in a contaminated mining technosol amended with biochar and planted with willow and ryegrass. J. Environ. Manag. 232, 117-130. https://doi.org/10.1016/j.jenvman.2018.11.021

Ouangrawa, M., Molson, J., Aubertin, M., Bussière, B., Zagury, G.J., 2009. Reactive transport modelling of mine tailings columns with capillarity-induced high water saturation for preventing sulfide oxidation. Appl. Geochem. 24, 1312–1323. https://doi.org/10.1016/j.apgeochem.2009.04.005

Pabst, T., Molson, J., Aubertin, M., Bussière, B., 2017. Reactive transport modelling of the hydro-geochemical behaviour of partially oxidized acid-generating mine tailings with a monolayer cover. Appl. Geochem. 78, 219–233. https://doi.org/10.1016/j.apgeochem.2017.01.003

Palandri, J.L., Kharaka, Y.K., 2004. A Compilation of Rate Parameters of Water-Mineral Interaction Kinetics for Application to Geochemical Modeling (No. 2004–1068).

Park, D.-U., Kim, D.-S., Yu, S.-D., Lee, K.-M., Ryu, S.-H., Kim, S.-G., Yang, W.-H., Park, D.-Yong., Hong, Y.-S., Park, J.-D., Lee, B.-K., Moon, J.-D., Sakong, J., Ahn, S.-C., Ryu, J.-M., Jung, S.-W., 2014. Blood levels of cadmium and lead in residents near abandoned metal mine areas in Korea. Environ. Monit. Assess. 186, 5209–5220. https://doi.org/10.1007/s10661-014-3770-1

Parkhurst, D.L., Appelo, C.A.J., 2013. Description of input and examples for PHREEQC version 3: a computer program for speciation, batch-reaction, one-dimensional transport, and inverse geochemical calculations (Report No. 6-A43), Techniques and Methods. Reston, VA. https://doi.org/10.3133/tm6A43

Pascaud, G., Leveque, T., Soubrand, M., Boussen, S., Joussein, E., Dumat, C., 2014. Environmental and health risk assessment of Pb, Zn, As and Sb in soccer field soils and sediments from mine tailings: solid speciation and bioaccessibility. Environ. Sci. Pollut. Res. 21, 4254–4264. https://doi.org/10.1007/s11356-013-2297-2

Plummer, L.N., Wigley, T.M.L., Parkhurst, D.L., 1978. The kinetics of calcite dissolution in CO 2 -water systems at 5 degrees to 60 degrees C and 0.0 to 1.0 atm CO_2. Am. J. Sci. 278, 179–216. https://doi.org/10.2475/ajs.278.2.179

Raines, M.A., Dewers, T.A., 1997. Mixed transport/reaction control of gypsum dissolution kinetics in aqueous solutions and initiation of gypsum karst. Chem. Geol. 140, 29–48. https://doi.org/10.1016/S0009-2541(97)00018-1

Roussel, C., Néel, C., Bril, H., 2000. Minerals controlling arsenic and lead solubility in an abandoned gold mine tailings. Sci. Tot. Environ. 263, 209–219. https://doi.org/10.1016/S0048-9697(00)00707-5

Sánchez-Chardi, A., Marques, C.C., Nadal, J., da Luz Mathias, M., 2007. Metal bioaccumulation in the greater white-toothed shrew, Crocidura russula, inhabiting an abandoned pyrite mine site. Chemosphere 67, 121–130. https://doi.org/10.1016/j.chemosphere.2006.09.009

Smith, A.M.L., Dubbin, W.E., Wright, K., Hudson-Edwards, K.A., 2006. Dissolution of lead- and lead–arsenic-jarosites at pH 2 and 8 and 20 °C: Insights from batch experiments. Chem. Geol. 229, 344–361. https://doi.org/10.1016/j.chemgeo.2005.11.006

Stotzky, G., 1965. Microbial Respiration, in: Norman, A.G. (Ed.), Agronomy Monographs. American Society of Agronomy, Soil Science Society of America, Madison, WI, USA, 1550–1572. https://doi.org/10.2134/agronmonogr9.2.c62

Sumner, M.E., 2000. Beneficial use of effluents, wastes, and biosolids. Commun. Soil Sci. Plant Anal. 31, 1701–1715. https://doi.org/10.1080/00103620009370532

Thienpont, J.R., Korosi, J.B., Hargan, K.E., Williams, T., Eickmeyer, D.C., Kimpe, L.E., Palmer, M.J., Smol, J.P., Blais, J.M., 2016. Multi-trophic level response to extreme metal contamination from gold mining in a subarctic lake. Proc. R. Soc. B 283, 20161125. https://doi.org/10.1098/rspb.2016.1125

Thouin, H., Norini, M.-P., Le Forestier, L., Gautret, P., Motelica-Heino, M., Breeze, D., Gassaud, C., Battaglia-Brunet, F., 2019. Microcosm-scale biogeochemical stabilization of Pb, As, Ba and Zn in mine tailings amended with manure and ochre. Appl. Geochem. 111, 104438. https://doi.org/10.1016/j.apgeochem.2019.104438

Tipping, E., Hurley, M.A., 1992. A unifying model of cation binding by humic substances. Geochim. Cosmochim. Acta 56, 3627–3641. https://doi.org/10.1016/0016-7037(92)90158-F

Wahlström, M., Laine-Ylijok, J., Kaartinen, T., Hjelmar, O., Bendz, D., 2009. Acid Neutralization Capacity of Waste–Specification of Requirement Stated in Landfill Regulations. Nordic Council of Ministers.

Walter, A.L., Frind, E.O., Blowes, D.W., Ptacek, C.J., Molson, J.W., 1994. Modeling of multicomponent reactive transport in groundwater: 2. Metal mobility in aquifers impacted by acidic mine tailings discharge. Water Resour. Res. 30, 3149–3158. https://doi.org/10.1029/94WR00954

Weber, P.A., Thomas, J.E., Skinner, W.M., Smart, R.St.C., 2005. A methodology to determine the acid-neutralization capacity of rock samples. Can. Miner. 43, 1183–1192. https://doi.org/10.2113/gscanmin.43.4.1183

Welch, S.A., Kirste, D., Christy, A.G., Beavis, F.R., Beavis, S.G., 2008. Jarosite dissolution II—Reaction kinetics, stoichiometry and acid flux. Chem. Geol. 254, 73–86. https://doi.org/10.1016/j.chemgeo.2008.06.010

Wolkersdorfer, C., Bowell, R., 2004. Contemporary Reviews of Mine Water Studies in Europe. Mine Water Environ. 23, 161–161. https://doi.org/10.1007/s10230-004-0059-6

Zhang, P., Ryan, J.A., 1998. Formation of Pyromorphite in Anglesite-Hydroxyapatite Suspensions under Varying pH Conditions. Environ. Sci. Technol. 32, 3318–3324. https://doi.org/10.1021/es980232m

Zhu, C., Anderson, G.M., Burden, D.S., 2002. Natural Attenuation Reactions at a Uranium Mill Tailings Site, Western U.S.A. Ground Water 40, 5–13. https://doi.org/10.1111/j.1745-6584.2002.tb02486.x

Zornoza, R., Faz, Á., Carmona, D.M., Acosta, J.A., Martínez-Martínez, S., de Vreng, A., 2013. Carbon mineralization, microbial activity and metal dynamics in tailing ponds amended with pig slurry and marble waste. Chemosphere 90, 2606–2613. https://doi.org/10.1016/j.chemosphere.2012.10.107

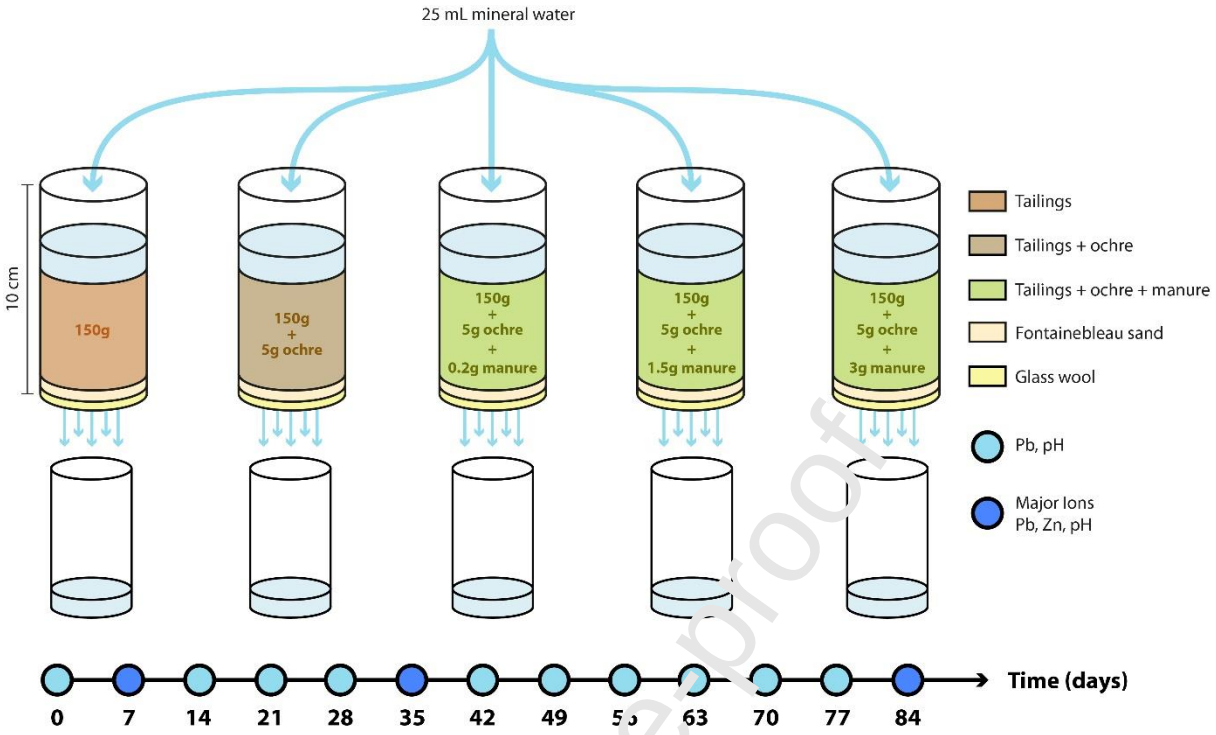

Fig. A.1. Schematic diagram of the leaching experiments.

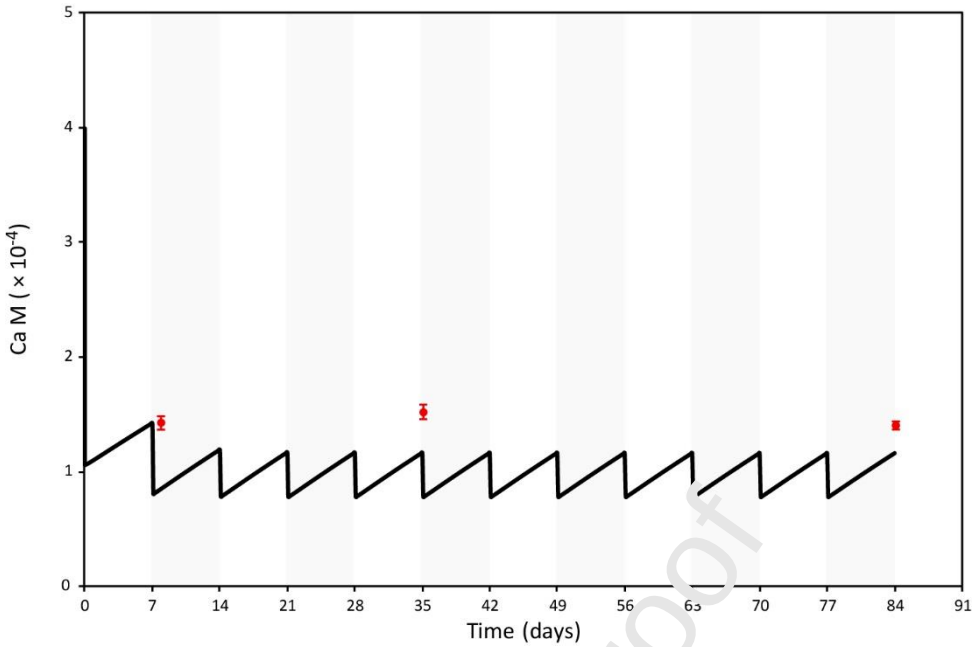

Fig. A.2. Evolution with time of Ca concentration in the case of leaching experiments with tailings without amendments. Red dots correspond to experimental data (Thouin et al., 2019), and solid line to calculated values.

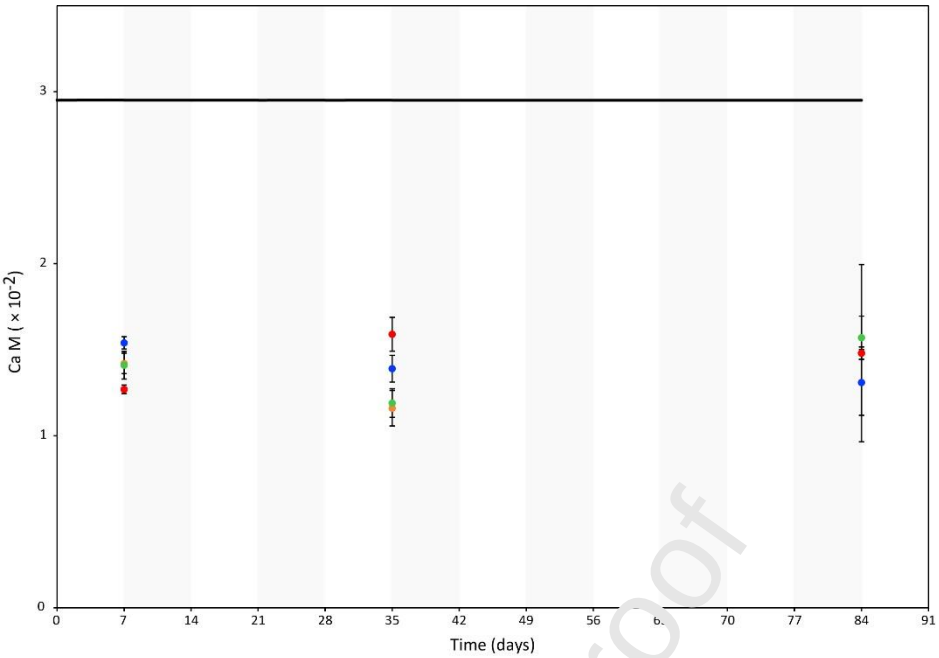

Fig. A.3. Evolution with time of Ca concentration in the case of leaching experiments with tailings with amendments. The solid line corresponds to calculated values, and dots to experimental data (Thouin et al., 2019): orange dots for ochre only, green dots for ochre + 0.15wt% of manure, red dots for ochre + 1wt% of manure and blue dots for ochre + 2wt% of manure.

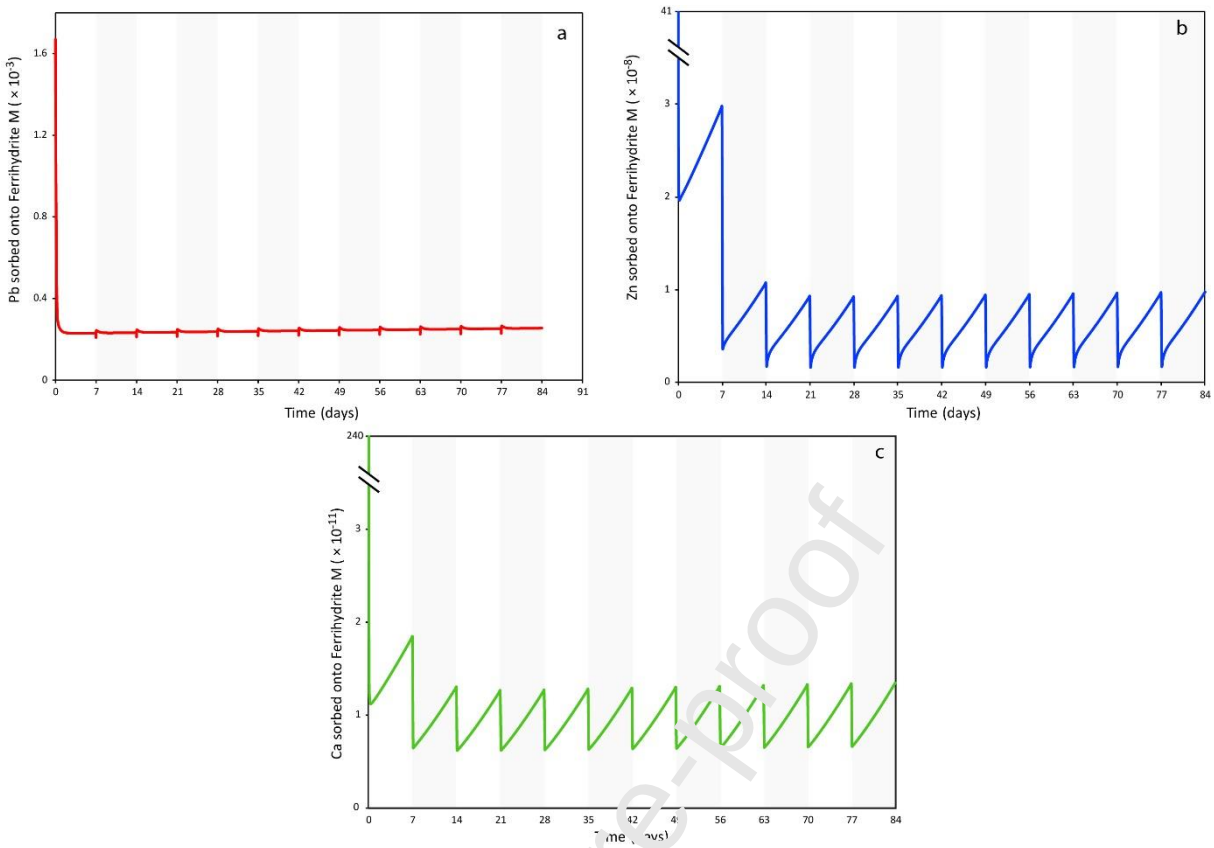

Fig. A.4. Modelling of surface sites occupation on ferrihydrite during the leaching experiment of tailings without amendment (T): (a) Pb concentration, (b) Zn concentration, (c) Ca concentration.

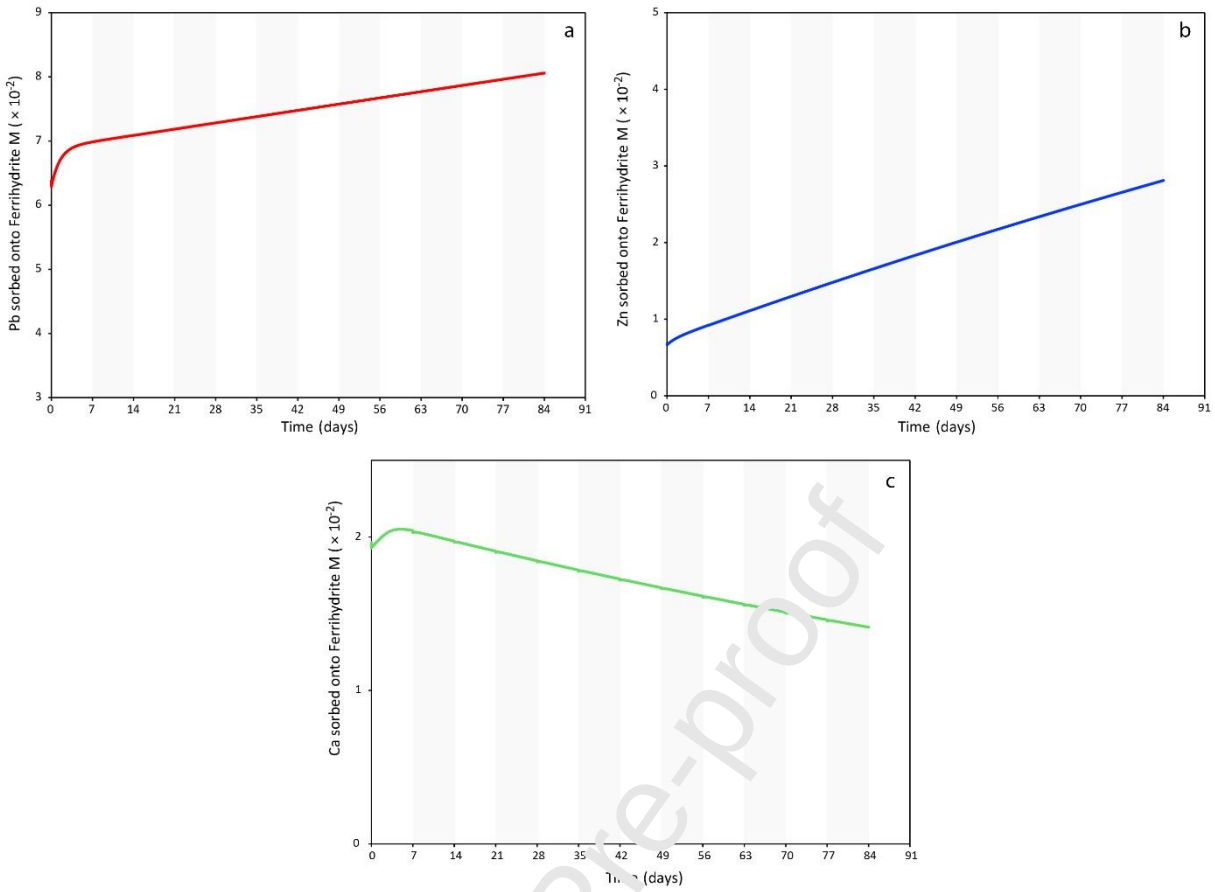

Fig. A.5. Modelling of surface sites occupation on ferrihydrite during the leaching experiment of tailings with ochre (TO): (a) Pb concentration, (b) Zn concentration, (c) Ca concentration.

Fig. A.6. Modelling of sorbed Pb, Zn and Ca concentrations during the leaching experiment for tailings amended with ochre and manure (TOM). Red lines correspond to 2wt% manure, blue lines to 1wt% manure, and green lines to 0.15wt% manure.

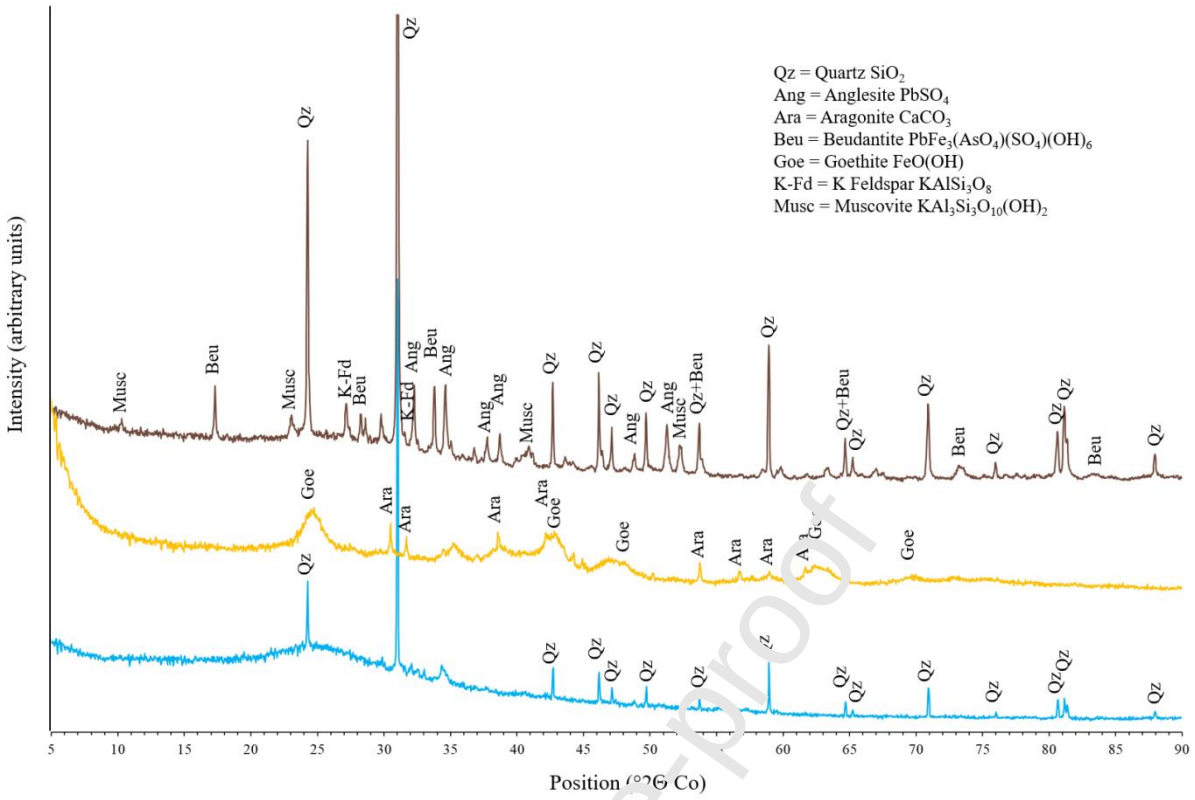

Fig. A.7. X-ray diffractograms of the tailings (brown line), the ochre (yellow line) and the manure (blue line), respectively.

Table A.1

Surface protonation reactions used for ferrihydrite in the simulations.

Sites	Density (mol/mol ferrihydrite)	Reaction	Log K[a]
Strong	0.005	$Hfo\_sOH + H^+ \leftrightharpoons Hfo\_sOH_2^+$	7.29
		$Hfo\_sOH \leftrightharpoons Hfo\_sO^- + H^+$	-8.93
Weak	0.2	$Hfo\_wOH + H^+ \leftrightharpoons Hfo\_wOH_2^+$	7.29
		$Hfo\_wOH \leftrightharpoons Hfo\_wO^- + H^+$	-8.93

[a] Log K values from Dzombak and Morel (1990).

Table A.2

Surface complexation reactions used for Pb, Zn and Ca in the simulations

Reactions	Log K[a]
$Hfo\_sOH + Pb^{2+} \leftrightharpoons Hfo\_sOPb^{+} + H^{+}$	4.65
$Hfo\_wOH + Pb^{2+} \leftrightharpoons Hfo\_wOPb^{+} + H^{+}$	0.3
$Hfo\_sOH + Zn^{2+} \leftrightharpoons Hfo\_sOZn^{+} + H^{+}$	0.99
$Hfo\_wOH + Zn^{2+} \leftrightharpoons Hfo\_wOZn^{+} + H^{+}$	-1.99
$Hfo\_sOH + Ca^{2+} \leftrightharpoons Hfo\_sOHCa^{2+}$	4.97
$Hfo\_wOH + Ca^{2+} \leftrightharpoons Hfo\_wOCa^{+} + H^{+}$	-5.85

[a] Log K values from Dzombak and Morel (1990).

Table A.3

Surface reactions used for protonation and cation complexation on organic matter.

Reactions		References
Monodentate carboxylic sites	Log K_{MHA}	
$H\_aH = H\_a^- + H^+$	-1.59	Tipping and Hurley, 1992
$H\_bH = H\_b^- + H^+$	-2.70	
$H\_cH = H\_c^- + H^+$	-3.82	
$H\_dH = H\_d^- + H^+$	-4.93	
$H\_(a,b,c,d)H + Pb^{2+} = H\_(a,b,c,d)Pb^+ + H^+$	-0.81	
$H\_(a,b,c,d)H + Zn^{2+} = H\_(a,b,c,d)Zn^+ + H^+$	-1.70	Christensen and Christensen, 1999
$H\_(a,b,c,d)H + Ca^{2+} = H\_(a,b,c,d)Ca^+ + H^+$	-3.20	Lofts and Tipping, 2000
Monodentate phenolic sites	Log K_{MHB}	
$H\_eH = H\_e^- + H^+$	-8.88	Tipping and Hurley, 1992
$H\_fH = H\_f^- + H^+$	-8.72	
$H\_gH = H\_g^- + H^+$	-10.56	
$H\_hH = H\_h^- + H^+$	-12.40	
$H\_(e,f,g,h)H + Pb^{2+} = H\_(e,f,g,h)Pb^+ + H^+$	-3.04	
$H\_(e,f,g,h)H + Zn^{2+} = H\_(e,f,g,h)Zn^+ + H^+$	-4.90	Log K_{MHB} = 2.57 +1.38(Log K_{MHA})
$H\_(e,f,g,h)H + Ca^{2+} = H\_(e,f,g,n)Ca^+ + H^+$	-6.99	Log K_{MHB} = 2.57 +1.38(Log K_{MHA})
Bidentate sites	Log K_{MHAB}	
$H\_abH2 = H\_ab^{2-} + 2H^+$	-4.29	Tipping and Hurley, 1992
$H\_adH2 = H\_ad^{2-} + 2H^+$	-6.52	
$H\_bcH2 = H\_bc^{2-} + 2H^+$	-6.52	
$H\_cdH2 = H\_cd^{2-} + 2H^+$	-8.75	
$H\_afH2 = H\_af^{2-} + 2H^+$	-10.31	
$H\_ahH2 = H\_ah^{2-} + 2H^+$	-13.99	

$H\_beH2 = H\_be^{2-} + 2H^{+}$	-9.58	
$H\_bgH2 = H\_bg^{2-} + 2H^{+}$	-13.26	
$H\_cfH2 = H\_cf^{2-} + 2H^{+}$	-12.54	
$H\_chH2 = H\_ch^{2-} + 2H^{+}$	-16.22	
$H\_deH2 = H\_de^{2-} + 2H^{+}$	-11.81	
$H\_dgH2 = H\_dg^{2-} + 2H^{+}$	-15.49	
$H\_(ab,ad,bc,cd)H2 + Pb^{2+} = H\_(ab,ad,bc,cd)Pb + 2H^{+}$	-1.62	$Log\ K_{MHAA} = 2(Log\ K_{MHA})$
$H\_(ab,ad,bc,cd)H2 + Zn^{2+} = H\_(ab,ad,bc,cd)Zn + 2H^{+}$	-3.40	
$H\_(ab,ad,bc,cd)H2 + Ca^{2+} = H\_(ab,ad,bc,cd)Ca + 2H^{+}$	-6.40	
$H\_(af,ah,….,de,dg)H2 + Pb^{2+} = H\_(af,ah,….,de,dg)Pb + 2H^{+}$	-1.85	$Log\ K_{MHAB} = Log\ K_{MHA} + Log\ K_{MHB}$
$H\_(af,ah,….,de,dg)H2 + Zn^{2+} = H\_(af,ah,….,de,dg)Zn + 2H^{+}$	-6.60	
$H\_(af,ah,….,de,dg)H2 + Ca^{2+} = H\_(af,ah,….,de,dg)Ca + 2H^{+}$	-10.20	

Declaration of interests

☒ The authors declare that they have no known competing financial interests or personal relationships that could have appeared to influence the work reported in this paper.

☐The authors declare the following financial interests/personal relationships which may be considered as potential competing interests: